Multi-level modeling of viscoelastic microcracked masonry

Amna Rekik, Thi Thu Nga Nguyen, Alain Gasser

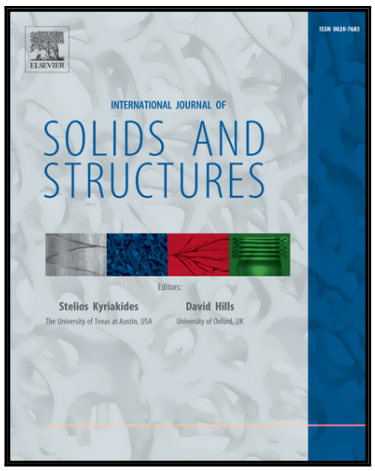

Multi-level modeling of viscoelastic microcracked masonry

Amna Rekik, Thi Thu Nga Nguyen, Alain Gasser

PII: S0020-7683(15)00464-3
DOI: 10.1016/j.ijsolstr.2015.11.002
Reference: SAS 8953

To appear in: *International Journal of Solids and Structures*

Received date: 8 April 2015
Revised date: 12 September 2015
Accepted date: 2 November 2015

Please cite this article as: Amna Rekik, Thi Thu Nga Nguyen, Alain Gasser, Multi-level modeling of viscoelastic microcracked masonry, *International Journal of Solids and Structures* (2015), doi: 10.1016/j.ijsolstr.2015.11.002

Highlights

- We propose a multi-level model to predict the orthotropic behaviour of cracked masonry
- This model relies on the coupling between Griffith's theory and homogenization methods
- Overall estimates of Cecchi & Taliercio model are softer than the Cecchi & Tralli's ones
- The Modified Maxwell model is relevant for the mortar's creep at short and long terms
- Both short and long terms, constant and time-dependent crack density were investigated

Multi-level modeling of viscoelastic microcracked masonry

Amna Rekik[1,*], Thi Thu Nga Nguyen[1], Alain Gasser[1]

[1] *Univ. Orléans, INSA-CVL, PRISME, EA*4229, 45072 *Orléans, France*
amna.rekik@univ-orleans.fr

Abstract

This paper provides multi-level modeling of microcracked viscoelastic masonries generally present in historical masonries or refractory linings. It is an extension of the Cecchi and Tralli [15] or Cecchi & Barbieri [13] and Cecchi & Taliercio [12] works for the typical Burgers and Modified Maxwell models followed by both undamaged and microcracked masonries. For the sake of simplicity and in order to provide rigorous analytical global estimates, only the mortar is assumed to be viscoelastic and microcracked. Bricks are assumed to be undamaged, elastic or quasi-rigid. The distribution of microcracks is assumed to be isotropic. The effective behaviour of the viscoelastic microcracked masonry is provided by two steps. The first one relies on the coupling between the Griffith's brittle fracture theory and linear mean-field homogenization scheme in order to account for the effect of microcracks on the macroscopic deformation of the mortar and establishes a linear relation between apparent macroscopic stress and strain. This step allows to easily and fast determine the effective creep function of the microcracked mortar without recourse to 'complex' or heavy numerical inversion of the Laplace-Carson transform. The second step is based on the coupling between asymptotic analysis and homogenization theory applied for a periodic masonry. The proposed models provide analytical solutions - explicit functions of the crack density parameter - for the effective orthotropic behaviour of a microcracked viscoelastic periodic masonry cell. This study proves that the Cecchi & Tralli's and Cecchi & Taliercio's extension estimates are close and that the later are softer. Such overall properties are used to perform finite element computations on a compressed masonry panel as a first application. These models allow then the prediction of mostly stressed and deformed areas in microcracked masonry structures. This study demonstrates that modeling a mortar (at its undamaged or microcracked state) with this Burgers formulation is only suitable for a masonry with too high values of the Maxwell's relaxation time otherwise it yields to vanishing effective properties with the increase of time and crack density leading thus to a premature collapse of the masonry. On the other hand, the Modified Maxwell model permits the masonry to preserve a certain resistance for every range value of Maxwell's relaxation time. These conclusions are valid for masonry either

with elastic or quasi-rigid undamaged bricks.

Keywords: Mean-field homogenization; Brittle fracture; Periodic homogenization; Viscoelasticity; Laplace-Carson transform; Masonry

---

Nomenclature

$\tilde{C}$ effective or homogeneous stiffness tensor
ϕ porosity volume fraction
A^p average of the strain localization tensor
A strain localization tensor
Ω_p pore space
u local displacement field
E macroscopic strain
ε^p average of the strain over the pore
S^E Eshelby tensor of the cavity function
A^p_{DL} dilute strain localization tensor A^p
w aspect ratio of an ellipsoidal cavity
$\tilde{C}^*$ effective stiffness in the symbolic space
$\dot{\varepsilon}$ local strain rate
$\dot{E}$ macroscopic strain rate
α ratio between mortar's and brick's dimensions
β ratio between brick's and mortar's stiffnesses
σ local stress field
Σ macroscopic stress field
σ_0 local stress field in pattern Y_b
ε_0 macroscopic stress field in pattern Y_b
$[u_0]$ displacement jump at interface Σ_I
Σ_I mortar joint interface in pattern Y_b
$[u]$ displacement jump between crack's two lips
J mortar's creep function
Y^* periodic cell of a running bond masonry
Y topological transferred pattern of the cell Y^*
Y^b periodic masonry Y^* with cohesive joints
K fourth-order stiffness tensor of cohesive joints
$[u^*]$ symbolic crack displacement jump
l radius of penny-shaped crack
d_c crack density parameter
k_s bulk's modulus of the undamaged matrix
μ_s shear's modulus of the undamaged matrix
ν_s undamaged matrix Poisson's ratio
k_l bulk's modulus of the spring
μ_l shear's modulus of the spring ($l = M$ or K)
η^s spherical bulk's viscosity of the dashpot
η^d deviatoric shear's viscosity of the dashpot
τ^s spherical relaxation time
τ^d deviatoric relaxation time
$< . >^r$ average over phase r of the quantity "."
i second-order identity tensor
I fourth-order identity tensor
J spherical fourth-order projector
K fourth-order stiffness tensor of mortar joint
μ_m shear moduli of mortar
a length of the brick
b height of the brick
e_h thickness of the bed joint
e_v thickness of the head joint
λ_m Lame's coefficient (plane stress)
λ^*_m Lame's coefficient (plane strain)

1. Introduction

Creep phenomenon and its effects are not only restricted to new structures but they involve also historical monuments as postulated in [44] and confirmed later in [6, 35]. Indeed heavy persistent compressive stresses added to the presence of aggressive environment (temperature/humidity conditions) and the self-weight of historical monuments induce stress redistribution and creep strains which can lead to damage accumulation and partial or total collapse of these monuments as it is the case of several famous examples: the Civic Tower of Pavia (Italy), the St. Magdalena bell-tower in Goch (Germany), the Noto and Monza Cathedrals (Italy) [35]. On the other hand, in the iron and steel industry, the refractory lining of furnaces made up of masonry with bricks and either mortared or dry (i.e. without mortar [1]) joints is often exposed to compressive (monotonic or cyclic) loads. These compressive loads result from constrained thermal expansion since the temperature inside these structures can reach 1650 degrees. This could induce creep behaviour and diffused damage due to initiation and propagation of micro-cracks mainly in the joints [3]. Generally, viscous behaviour of vitreous materials in gaz turbine engines has been modeled by temperature independently rheological models like Maxwell and the generalized Maxwell models [24]. Models with a temperature parameter have also been defined since the steady-state creep deformation of ceramics under sustained loading conditions normally exhibits a power-law stress-dependent behaviour [26, 2, 25, 30]. Traditionally, both tensile and compressive creep in ceramic materials have been characterized by an empirical creep equation that takes on the form of the Norton-Bailey-Arrhenius equation. Note that a thick mortar tends to decrease the stiffness of structure and increases the likelihood of the possible penetration of process materials into the joints, resulting in the deterioration of the lining. So, the use of thin mortar joint is appropriate and necessary in designing the refractory brick lining system.
Concerning the creep behaviour of traditional mortar, various rheological models namely the USBR, Feng, Ross, typical and modified versions of the Burgers and Modified-Maxwell models may be investigated [17, 28]. On the other hand, there exist several approaches accounting for damage in viscoelastic materials [28, 32]. Indeed, the approach presented in [32] is based on a coupling between continuum damage mechanics and viscoelasticity through the generalized Kelvin-Voigt model. Accordingly, a three-dimensional phenomenological model was developed to describe the long-term creep of gypsum rock. The main disadvantage of this model is that it requires experimental investigation [28] or computational efforts to resolve nonlinear equation [32] function of internal damage variables. In the works of Nguyen et al. [36, 38], the effective behaviour of microcracked linear viscoelastic concrete was derived from a combination of the Griffith's theory [27] and the Eshelby-based homogenization scheme [4]. The undamaged concrete was assumed to obey to the typical

Burgers model. In [17], an experimental study was carried in order to investigate the creep of masonry. A number of rheological models (USBR, Feng, Ross, typical Burgers, Modified Maxwell) are examined to assess their ability to predict the creep of masonry. It was proved that the Modified Maxwell model is the most accurate. According to this result, the Burgers model, namely a Maxwell system connected in series with a Kelvin-Voigt one, and the Modified Maxwell scheme (a parallel combination of the Maxwell model and a spring) models are adopted in this paper to describe the mortar joint's creep. Moreover, in the literature, little attention is devoted to the prediction of the macroscopic creep behaviour of masonry. In this context, Brooks, Cecchi & Tralli, Cecchi & Taliercio and Taliercio [8, 15, 12, 45] proposed models to predict creep coefficients according to the properties of each masonry constituent. These models are based on analytical or numerical homogenization using the finite elements method (FEM) in order to deduce the macroscopic creep of undamaged (without cracks) masonry. In the present study, the coupling between the Griffith's theory and the dilute scheme [4] will be applied to provide the effective behaviour of a micro-cracked mortar [36]. In a second step, the expressions proposed in [15, 12] are extended to determine the effective behaviour of a periodic microcracked viscoelastic masonry cell. It is worth noting that even the dilute scheme is useful for dilute concentrations of cracks, it has been demonstrated in [23, 22] that its estimates coincide with the Mori-Tanaka predictions and are close to the Ponte-Castañeda-Willis (PCW) estimates for $d_c \leq 0.15$). This result is valid for open and closed frictionless cracks. These global properties are used to compute the behaviour of a compressed wall as done in [15]. The main hypothesis adopted in this work are explicited in section 2 for both first and second steps based respectively on the approximation of the creep function of a microcracked non-aging linear viscoelastic mortar and the determination of the effective stiffness of a regular masonry with undamaged bricks and microcracked mortar joints with finite dimensions. The modified Maxwell and Burgers models followed by the rheology of undamaged mortar are recalled in section 3. The steps allowing the determination of the effective creep function of a microcracked linear viscoelastic mortar are explained in section 4. Section 5 provides a first application of the proposed Cecchi & Tralli and Cecchi & Taliercio extension models to a 2D masonry with microcracked viscoelastic hybrid mortar. This section studies the effects of crack density parameter, time and ratio between the bricks and mortar Young's moduli on the evolutions of mortar's creep function and masonry periodic cell's stiffness. At last, section 6 presents local and global mechanical fields predictions for a compressed masonry panel studied in [15]. In addition to the crack density parameter and time, this section studies the effects of the mortar's rheology model and panel's boundary conditions.

2. Main objective and hypothesis

The objective of this study is to evaluate the effective and local behaviour of masonries exhibiting nonlinear behaviours mainly viscoelastic at short and/or long times especially when they are subjected to severe or long term loading such as historical monuments or refractory masonry linings working under high temperatures. For undamaged state, this work enlarges the applications - USBR and Feng models - treated in the Cecchi & Tralli paper and the Generalized Maxwell model in the Cecchi & Taliercio work to the Modified Maxwell and typical Burgers rheological models. Moreover it is an extension of these models to microcracked viscoelastic masonries which considers apart the spherical and deviatoric parts of the creep behaviour unlike applications in [15]. Since this model provides stress distribution throughout studied masonry wall or structure with low computational efforts, it allows to predict cracked areas or failure zones mainly if compressive, tensile and shear masonry's strengths are beforehand known. For first applications and for the sake of simplicity, it can be assumed that only the mortar is a micro-cracked viscoelastic material [41, 31]. Its behaviour (at the undamaged state) obeys to the Modified Maxwell or typical Burgers models. The blocks or bricks are assumed to be undamaged and to have either a rigid or elastic isotropic behaviour. In the mortar, the cracks are assumed to be penny-shaped and to have an isotropic distribution. The proposed approach is based on two main steps. Firstly, the homogenization technique is applied in order to assess the effective behaviour of the micro-cracked mortar. The results of brittle fracture mechanics - the Griffith's theory - could be useful if we move from the real temporal space to the symbolic one due the Laplace-Carson (LC) transform. In the later space, the apparent behaviour of the mortar is linear elastic. This procedure allows the use of expressions available in the literature for the displacement's jump induced by the crack [36]. Assuming again that the displacement jump field depends linearly on the macroscopic stress, it is possible to define an effective linear behaviour for the micro-cracked mortar in the symbolic space. To determine the global behaviour in the real space time, it is possible to apply the inverse of the LC transform in some simple cases. It is then interesting to approach in the symbolic space, at least in short and long terms, the symbolic effective stiffness (or compliance) by an existing rheological model. For example, if the undamaged mortar behaves as the Modified Maxwell model, we try to approach the symbolic effective behaviour of the corresponding microcracked mortar by the same model. After validation of this approximation at short and long terms, the inversion of the apparent effective stiffness will be straightforward. Therefore, the effective behaviour of the micro-cracked viscoelastic mortar could be expressed in the real space time. In a second step, the global behaviour proposed for undamaged linear viscoelastic periodic masonries [15, 13, 12] is extended in this study for similar masonry cell with microcracks.

Basic steps followed by the proposed models - extension of the Cecchi & Tralli [15] and Cecchi & Taliercio [12] models to microcracked viscoelastic masonries - are summarized in Figure (1). Hereafter, it is proposed to explicit the main hypothesis adopted to carry out and perform the principle steps ((s_1) and (s_2)) of the proposed model.

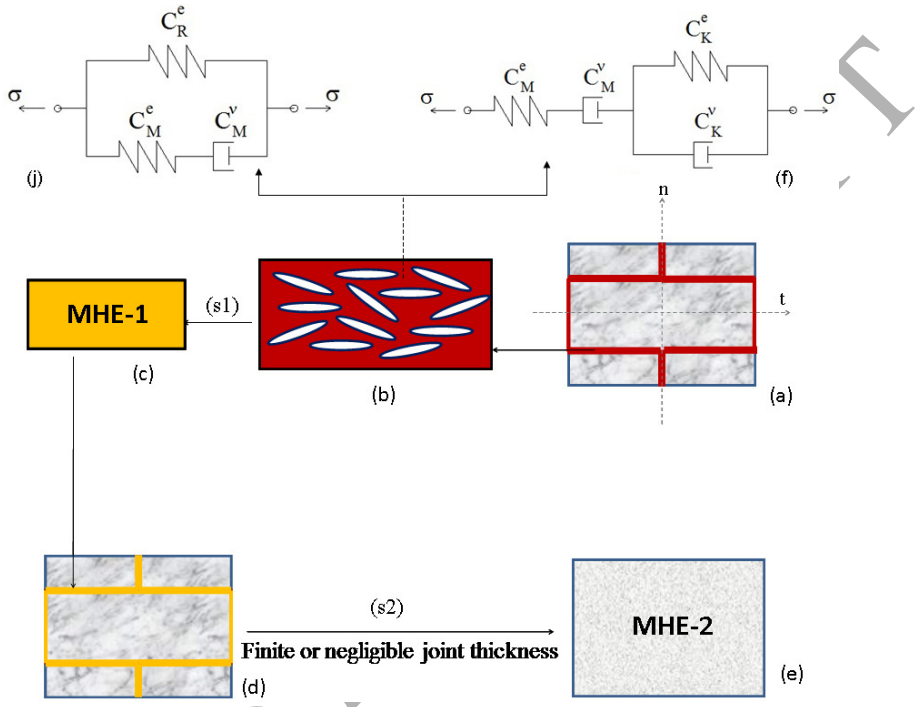

Figure 1: Main steps of the proposed model: (s_1) - approximation of the effective creep function knowing the effective properties of the homogeneous material MHE-1 (c) equivalent to the non-aging linear viscoelastic mortar (b) joints with isotropic distribution of cracks present in the periodic masonry cell (a) - and (s_2) based on two techniques: periodic homogenization (if dimensions of joints are finite [15, 13]) and asymptotic analysis (if these dimensions tend to 0 [14, 12]) in order to provide the effective stiffness of the homogeneous material MHE-2 (e) equivalent to the masonry's cell (d). The rheology of the mortar with penny-shaped micro-cracks follows either the Modified Maxwell (j) or typical Burgers (f) model.

2.1. Homogenization of a microcracked viscoelastic mortar: coupling between Griffith's theory and mean-field homogenization in the Laplace-Carson space

Let us firstly recall that the effective stiffness of an elastic porous medium with a homogeneous solid phase tensor C^s is:

$$\tilde{C} = C^s : (I - \phi A^p) \tag{1}$$

where A^p is the average of the strain localisation tensor $A(z)$ over the pore space Ω^p and ϕ is the porosity volume fraction. Classical estimates of A^p are based on the solution of the Eshelby single

ellipsoidal inhomogeneity problem. Indeed this inhomogeneity Ω_p is assumed to be embedded in an infinite homogeneous medium made up of an elastic material subjected to linear displacement boundary conditions of the form:

$$u(z) = E.z \quad \text{where} \quad z \to \infty \tag{2}$$

In that case, the strain ε^p in the inhomogeneity proves to be uniform. In the particular case of a cavity embedded in an infinite solid medium, ε^p is given by:

$$\varepsilon^p = (I - S^E)^{-1} : E \tag{3}$$

where S^E is the Eshelby tensor of the cavity function of the cavity's geometry and the bulk elasticity tensor C^s. According to equation (3), the dilute scheme's estimate of the localization tensor A^p reads:

$$A^p_{DL} = (I - S^E)^{-1} \tag{4}$$

For a flat spheroid - usual $3D$ crack model - of aspect ratio $w << 1$, the Eshelby tensor S^E is a function of w. Accordingly the components A^p_{iikl} and A^p_{ikik} of the tensor (4) are of the order of $1/w$ and therefore is the ratio of the normal strain ε_{nn} to the macroscopic strain E. Possible nonenegligible variations of $1/w$ is in contradiction with the assumption of linearity of the localization relationship (3). To overcome this difficulty, Deudé et al. [21] have proposed to consider the rate-type formulation of the problem i.e. the strain localisation tensor (3) should be replaced by a strain rate localization as in the following:

$$\dot{\varepsilon}(z) = A(z) : \dot{E}$$

Similarly, the rate-type formulation of the Eshelby problem (3) for a spheroidal cavity reads:

$$\dot{\varepsilon^p} = (I - S^E(w))^{-1} : \dot{E} \tag{5}$$

Recall that w here refers to the aspect ratio in the current configuration of the spheroidal cavity. Such hypothesis implies that the use of A^p in the homogenized stiffness (1) leads to an estimate of the tangent effective stiffness. Moreover, since the crack porosity ϕ is proportional to w [21], the tangent effective stiffness is mathematically independent of w. This renders the effective behaviour linear elastic. Note that the rate-type hypothesis is indispensable [21] to also avoid troubles related to possible large strain in the direction normal to the crack.

On the other hand, the extension of the linear homogenization schemes to non-aging viscoelasticity is based on the Laplace-Carson (LC) transform [42, 40]. The effective stiffness $\tilde{C} =< C : A >$ becomes

$$\tilde{C^*} =< C^* : A > \tag{6}$$

in the LC space where C^* is the apparent elastic stiffness. The presence of microcracks implies the existence of nonlinearity at the local scale in the relationship between the crack strain and the macroscopic strain. Accordingly the homogenization of a viscoelastic cracked medium is not as straightforward as (6). The basic idea consists in anticipating that both the microscopic strain field and the displacement discontinuity vectors $[u]_i$ linearly depend on the macroscopic stress. Such an hypothesis, confirmed by [36], justifies the use of the LC transform which can be applied to the macroscopic strain related to the microscopic strain and the displacement discontinuity vectors $[u]_i$ between two lips of crack.

2.2. Homogenization of regular masonry with viscoelastic mortar joints: coupling between asymptotic analysis and periodic homogenization in the real temporal space

Since the procedure explained in the previous paragraph (see section (2.1)) provides the apparent creep function J^* of the microcracked viscoelastic mortar, it is possible to derive the real creep function using an appropriate (analytical due to the Bromwich integral defined in the complex plane by $f(t) = \frac{1}{2\pi}\int \frac{f^*(p)}{p} e^{pt} dp$ [5] or numerical as the collocation [40] or multi-data [18] methods) inversion procedure of the LC transform.

2.2.1. ***Linear elastic case***

Classically, to determine the global behaviour of regular masonry with linear elastic constituents, it is useful to apply periodic homogenization technique. For that purpose, Cecchi and Rizzi [11], De Felice [19, 20] and Cecchi and Sab [14] have proposed to apply asymptotic homogenization technique with a perturbative analysis as a function of several parameters: ε_0 that defines the relationship between the overall dimensions of the element and those of the characteristic pattern, α which defines the relationship between the dimension of the mortar joint and that of the characteristic pattern and β defining the ratio of the mortar stiffness to the brick stiffness in order to provide constitutive functions depending on the said parameters. Besides these authors have investigated the obtained solutions as these parameters tend towards zero which is frequently the case for the bed joints. These studies are motivated by the fact that a mortar in historical masonry is much more deformable than the block and that its thickness is often negligible compared to the dimensions of the blocks. The homogenized stiffness tensor $A^{i,j}$ is computed on Y^* by solving the following auxiliary problem on the periodic linear elastic masonry pattern Y^* (see Figure (2)-a).

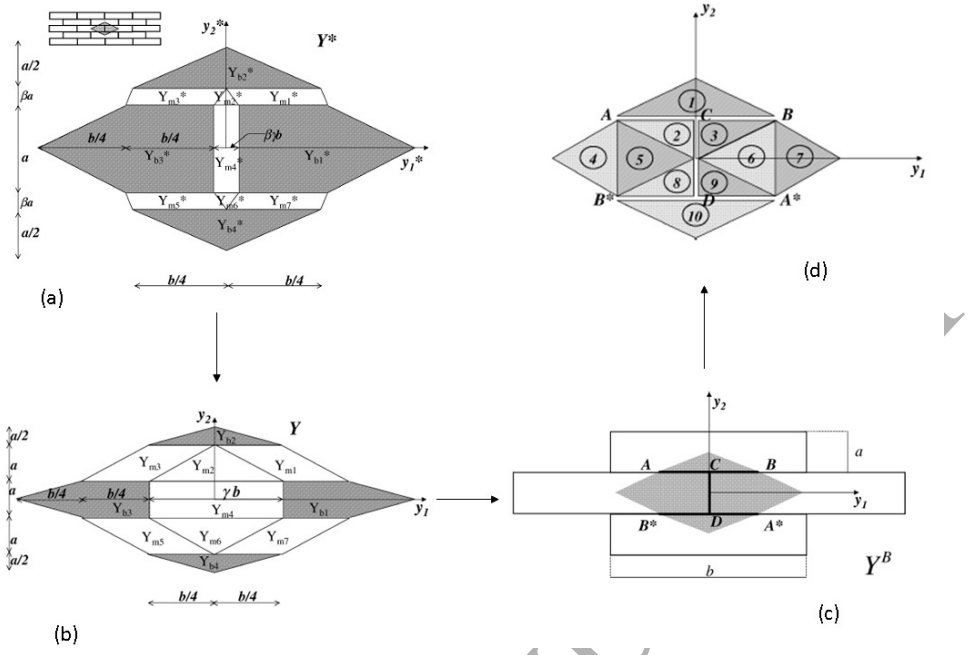

Figure 2: Running bond masonry: finite element discretization (d) and topological transformations (patterns Y (b), Y^B with mortar joints assimilated to interfaces or surface discontinuities (c)) of the characteristic elementary pattern Y^* (a) followed by Cecchi and Sab in [14].

$$\begin{cases} div(\sigma^*) = 0 \\ \varepsilon^*(y^*) = E + sym(grad\, u^{*per}) \\ \sigma^* = a^{i,j} : \varepsilon(y^*) \\ \sigma^*.n \quad \text{anti-periodic on} \quad \partial Y^* \\ u^{*per} \quad \text{periodic on} \quad \partial Y^* \end{cases} \quad \text{where} \quad a^{i,j}(y^*) = \begin{cases} a^b \quad \text{for} \quad y^* \in \text{block} \\ a^m \quad \text{for} \quad y^* \in \text{mortar} \end{cases} \tag{7}$$

Here a^b and a^m are respectively the elastic constitutive functions pertaining to the blocks and mortar. σ^* and ε^* are respectively the local stress and strain in the cell Y^*. n is a unit vector normal to the boundary ∂Y^* of this cell and u^* is the local displacement field of a point M pertaining to this cell. For a macroscopic strain E, it follows that: $\Sigma = \langle \sigma^* \rangle_{Y^*} = A^{\alpha,\beta} : E$.

After topological transformation of periodic pattern Y^* (see pattern Y in Figure (2)-b)) and assuming that $\lim \alpha(\beta)\beta^{-1} = w_0 \neq 0$, that means for periodic masonry with cohesive joints, the authors have shown that the auxiliary problem (7) can be rewritten as follows with reference to the pattern Y^b

(see Figure (2)-c)

$$\begin{cases} div(\sigma^0) = 0 \\ \varepsilon^0(y) = E + \nabla^s u^0 \\ \sigma^0 = A^b : \varepsilon^0(y) \end{cases} \quad \text{with boundary conditions} \quad \begin{cases} \sigma^0.n \text{ anti-periodic on } \partial Y^b \\ u_0 \quad \text{periodic on} \quad \partial Y^b \\ [u_0] \neq 0 \text{ discontinuous on } \Sigma_I \\ [\sigma^0.n] = 0 \text{ continuous on } \Sigma_I \\ \sigma^0.n = K\,[u_0] \text{ constitutive relation on } \Sigma_I \end{cases} \tag{8}$$

where σ_0 and ε_0 are local stress and strain fields in the pattern Y_b. n is the unit vector in the y_1 and y_2 middle planes of the $Y-$REV, Σ_I is the interface and $[u_0]$ is the jump in displacement field at Σ_I and the fourth-order tensor K is given by

$$K_h \approx \frac{1}{e_h}(\mu_M I + (\mu_M + \lambda_M) n \otimes n), \quad K_v \approx \frac{1}{e_v}(\mu_M I + (\mu_M + \lambda_M) n \otimes n) \tag{9}$$

assuming isotropic behaviour of mortar [29]. The resolution of the auxiliary problem (8) in terms of the variables (σ_0, u_0) allows to determine the homogenized stiffness $\tilde{A}$ in the following form by reference to the patternY_b [14]

$$\begin{aligned} \tilde{A}_{1111} &= \frac{\left(K' C^b_{1111} + B\frac{e_h}{a}\right)\left(4K'\frac{e_h}{a} + \frac{b}{a}K''\frac{e_v}{a}\right)}{4\left(\frac{e_h}{a}\right)^2 \frac{e_v}{b}B + C^b_{1111}\frac{e_h}{a}C + K'D}, \quad \tilde{A}_{2222} = K' \frac{K' C^b_{2222} + B\frac{e_v}{b}}{\frac{e_v}{b}\frac{e_h}{a}B + K' C^b_{2222}\left(\frac{e_h}{a} + \frac{e_v}{b}\right) + K'^2} \\ \tilde{A}_{1122} &= K' C^b_{1122} \frac{\left(4K'\frac{e_h}{a} + \frac{b}{a}K''\frac{e_v}{a}\right)}{4\left(\frac{e_h}{a}\right)^2 \frac{e_v}{b}B + C^b_{1111}\frac{e_h}{a}C + K'D}, \quad \tilde{A}_{1212} = C^b_{1212}K'' \frac{\left(K'\frac{e_v}{b} + 4\frac{a}{b}K''\frac{e_h}{b}\right)}{C^b_{1212}\frac{e_h}{a}F + K''G} \end{aligned} \tag{10}$$

where $B = \left(C^b_{1111}\right)^2 - \left(C^b_{1122}\right)^2$, $C = 4K'\frac{e_h}{a} + \frac{e_v}{a}K''\frac{b}{a} + 4K'\frac{e_v}{b}$, $D = 4K'\frac{e_h}{a} + \frac{e_v}{a}K''\frac{b}{a}$,
$F = K'\frac{e_v}{b} + 4K''\left(\frac{e_h}{b}\frac{a}{b} + \left(\frac{a}{b}\right)^2\frac{e_v}{b}\right)$, $G = K'\frac{e_v}{b} + 4\frac{e_h}{b}K''\frac{a}{b}$, $K' = 2\mu_m + \lambda_m$ (plane strain)
or $K' = 2\mu_m + \lambda^*_m$ (plane stress) and $K'' = \mu_m$ or equivalently

$$\begin{aligned} K'_h &= \frac{E^m}{(1-(\nu^m_h)^2)}, & K'_v &= \frac{E^m}{(1-(\nu^m_v)^2)} && \text{(plane stress)} \\ K'_h &= \frac{(1-\nu^m_h)E^m}{(1+\nu^m_h)(1-2\nu^m_h)}, & K'_v &= \frac{(1-\nu^m_v)E^m}{(1+\nu^m_v)(1-2\nu^m_h)} && \text{(plane strain)} \\ K''_h &= \frac{E^m}{2(1+\nu^m_h)}, & K''_v &= \frac{E^m}{2(1+\nu^m_v)} \end{aligned} \tag{11}$$

since $\mu = \frac{E}{2(1+\nu)}$, $\lambda = \frac{\nu\, E}{(1+\nu)(1-2\nu)}$ and $\lambda^* = \frac{\nu\, E}{(1-\nu^2)}$. a and b are respectively the height and length of the brick in Y^b. e_h and e_v are thicknesses of the mortar joints in the horizontal and vertical

directions, respectively. These results are, in the limit, perfectly consistent with those obtained by De Felice [20] in the case of rigid blocks and joints modeled as an elastic interface. The analytical solution (10) is accurate when ratios between bricks and joints mortar dimensions tend toward 0 which is generally the case for bed joints. It is less accurate in the vertical direction since e_v/h_b is generally not negligible compared to e_h/l_b. Motivated by this reason, Cecchi & Barbieri and Cecchi & Tralli have proposed an alternative analytical solution valid for finite joint thickness. Indeed, following the procedure of Cecchi and Tralli [15], it is noted that the homogenized moduli for an elastic brick and joint are obtained in the pattern Y, and not in Y_b as done in Cecchi and Sab [14]. The joint thickness is taken into account in the following mathematical procedure

$$E.(\tilde{a}^H\, E) \leq E.(\tilde{A}\, E) \leq \min\left\{E.(\tilde{A}^H\, E), E.(\tilde{A}^R\, E)\right\} \tag{12}$$

where $\tilde{a}^H$ is the homogenized 2D elasticity tensor obtained with plane stress in the bricks and 2D restriction of K at the plane strain interface in the mortar. $\tilde{A}^H$ is the homogenized plane strain elasticity tensor i.e. with plane strain hypothesis in both blocks and mortar. $\tilde{A}^R$ is the homogenized in-plane tensor defined by:

$$(\tilde{A}^R)^{-1} = (A^{b*})^{-1} + (A^F)^{-1} \tag{13}$$

where A^{b*} is the plane stress elasticity tensor of blocks and A^F is the homogenized membrane tensor for rigid blocks connected by elastic interfaces. The homogenized tensor $\tilde{A}^R$ reads [15]

$$\begin{aligned}
\tilde{A}^R_{1111} &= \frac{\left(K'_h C^b_{1111} + B\dfrac{e_h}{a+e_h}\right)\left(4K'_v\dfrac{e_h}{a+e_h} + \dfrac{b+e_v}{a+e_h}K''_h\dfrac{e_v}{a+e_h}\right)}{4\left(\dfrac{e_h}{a+e_h}\right)^2\dfrac{e_v}{b+e_v}B + C^b_{1111}\dfrac{e_h}{a+e_h}C + K'_h D},\\
\tilde{A}^R_{2222} &= K'_h\frac{\left(4K'_v\dfrac{e_h}{a+e_h} + \dfrac{b+e_v}{a+e_h}K''_h\dfrac{e_v}{a+e_h}\right)C^b_{1111} + B\dfrac{e_h}{a+e_h}\dfrac{e_v}{a+e_v}}{4\left(\dfrac{e_h}{a+e_h}\right)^2\dfrac{e_v}{b+e_v}B + C^b_{1111}\dfrac{e_h}{a+e_h}C + K'_h D},\\
\tilde{A}^R_{1122} &= K'_h C^b_{1122}\frac{\left(4K'_v\dfrac{e_h}{a+e_h} + \dfrac{b+e_v}{a+e_h}K''_h\dfrac{e_v}{a+e_h}\right)}{4\left(\dfrac{e_h}{a+e_h}\right)^2\dfrac{e_v}{b+e_v}B + C^b_{1111}\dfrac{e_h}{a+e_h}C + K'_h D},\\
\tilde{A}^R_{1212} &= C^b_{1212}K''_h\frac{\left(K'_h\dfrac{e_v}{b+e_v} + 4\dfrac{a+e_h}{b+e_v}K''_h\dfrac{e_h}{b+e_v}\right)}{C^b_{1212}\dfrac{e_h}{a+e_h}F + 4K''_h G}
\end{aligned} \tag{14}$$

where, here $C = 4K'_v\dfrac{e_h}{a+e_h} + \dfrac{e_v}{a+e_h}K''_h\dfrac{b+e_v}{a+e_h} + 4K'_h\dfrac{a}{a+e_h}\dfrac{e_v}{b+e_v}$. The differences between equations (14) and those obtained by Cecchi and Sab [14] (see equations (10)) lie in the ratio $\dfrac{e_v}{b}$ and $\dfrac{e_h}{a}$, which

are substituted respectively by $\frac{e_v}{b+e_v}$ and $\frac{e_h}{a+e_h}$, in the components $\tilde{A}^R_{2222}$, $\tilde{A}^R_{1212}$ and the coefficients C (mentionned above) and D. In the Cecchi & Barbieri's paper: $D = \frac{a}{a+e_h}\left(4K'\frac{e_h}{a+e_h} + \frac{(b+e_v)}{(a+e_h)}K''\frac{e_v}{a+e_h}\right)$,

$$\begin{aligned}\tilde{A}^R_{2222} &= K'\frac{K'C^b_{2222} + B\dfrac{e_v}{b+e_v}}{\dfrac{e_v}{b+e_v}\dfrac{e_h}{a+e_h}B + K'C^b_{2222}\left(\dfrac{e_h}{a+e_h}+\dfrac{e_v}{b+e_v}\right) + K'^2},\\ \tilde{A}^R_{1212} &= C^b_{1212}K''\frac{\left(K'\dfrac{e_v}{b+e_v} + 4\dfrac{a+e_h}{b+e_v}K''\dfrac{e_h}{b+e_v}\right)}{C^b_{1212}\dfrac{e_h}{a+e_h}F + 2K''G}.\end{aligned} \tag{15}$$

2.2.2. ***Extension to viscoelatic case***

For the viscoelastic periodic problem, the auxiliary problem (7) related to the elastic constituents can be rewritten as follows by reference to the periodic pattern Y^*

$$\begin{cases} \dot{E} + \varepsilon(\dot{u}^{per}) = \varepsilon(\dot{u}) \\ div(\sigma(t)) = 0 \\ \sigma(t).n \quad \text{anti-periodic on} \quad \partial Y \\ u^{per} \quad \text{periodic on} \quad \partial Y \\ \langle\sigma(t)\rangle = \Sigma(t) \end{cases} \tag{16}$$

Here, $\sigma(t)$ is the microscopic stress tensor state; $\varepsilon(\dot{u}(y))$ is the microscopic strain tensor state; u^{per} is the periodic displacement field and $\dot{E}$ is the macroscopic in-plane strain tensor rate.

Since in the Cecchi & Tralli work, the hypothesis of cohesive joints was also adopted, an asymptotic auxiliary problem (similar to equations (8)) can be written with reference to the pattern Y^b. The mortar appears merely as a boundary condition. In that case, assuming also that the viscoelastic mortar is isotropic, then the K tensor can be rewritten as function of the viscous function of the mortar, i.e.:

$$\begin{aligned} K_h(t) &= \frac{1}{e_h}\left(\frac{E^m_h(1+\phi^m_h(t))}{2(1+\nu_m)}I + \left(\frac{E^m_h(1+\phi^m_h(t))}{2(1+\nu_m)} + \frac{\nu_m E^m_h(1+\phi^m_h(t))}{(1+\nu_m)(1-2\nu_m)}\right)(n\otimes n)\right)K_v(t)\\ &= \frac{1}{e_v}\left(\frac{E^m_v(1+\phi^m_v(t))}{2(1+\nu_m)}I + \left(\frac{E^m_v(1+\phi^m_v(t))}{2(1+\nu_m)} + \frac{\nu_m E^m_v(1+\phi^m_v(t))}{(1+\nu_m)(1-2\nu_m)}\right)(n\otimes n)\right)\end{aligned} \tag{17}$$

where the K tensor has a diagonal form in this case. $K = K_h$ for the horizontal interface and $K = K_v$ for the vertical interface.

If only the mortar is assumed to be viscoelastic such that its stiffness tensor reads $A^m(t) = A^m(1+$

$\phi_m(t)$), the periodic constitutive function $A^{i,j}$ is similar to that shown in (14) but by substituting the Young's modulus E^m by the inverse creep function $J_m^{-1}(t) = E^m(1+\phi_m(t))$. It is noted that here only the Young's modulus is assumed to be a function of viscosity; the only characteristic parameters for mortar are the bulk modulus and shear modulus, rather than the Poisson's ratio.

For a microcracked mortar, it is proposed in step (s_2) (see Figure (1)) to estimate the effective moduli of the homogeneous equivalent material MHE-2 (see Figure (1)-e). These properties could be deduced from the macroscopic plane stress law $\Sigma = \tilde{C} : \bar{\varepsilon}$ or equivalently $\bar{\varepsilon} = \tilde{S} : \Sigma$ which reads

$$\begin{pmatrix} \bar{\varepsilon}_{nn} \\ \bar{\varepsilon}_{tt} \\ 2\bar{\varepsilon}_{nt} \end{pmatrix} = \begin{pmatrix} \frac{1}{\tilde{E}_n} & -\frac{\tilde{\nu}_{nt}}{\tilde{E}_n} & 0 \\ -\frac{\tilde{\nu}_{tn}}{\tilde{E}_t} & \frac{1}{\tilde{E}_t} & 0 \\ 0 & 0 & \frac{1}{\tilde{\mu}_{nt}} \end{pmatrix} \begin{pmatrix} \Sigma_{nn} \\ \Sigma_{tt} \\ \Sigma_{nt} \end{pmatrix} \tag{18}$$

where $\tilde{S}$ and $\tilde{C}$ are respectively the effective compliance and stiffness of the masonry periodic cell. Accordingly

$$\begin{aligned} &\frac{1}{\tilde{E}_t(t,d_c)} = \frac{\tilde{C}_{nn}}{\tilde{C}_{nn}\tilde{C}_{tt} - \tilde{C}_{ttnn}\tilde{C}_{nntt}}, \quad \tilde{\nu}_{nt}(t,d_c) = \frac{\tilde{C}_{nntt}}{\tilde{C}_{tt}}, \quad \tilde{\nu}_{tn}(t,d_c) = \frac{\tilde{C}_{ttnn}}{\tilde{C}_{nn}} \\ &\frac{1}{\tilde{E}_n(t,d_c)} = \frac{\tilde{C}_{tt}}{\tilde{C}_{nn}\tilde{C}_{tt} - \tilde{C}_{ttnn}\tilde{C}_{nntt}}, \quad \tilde{\mu}_{nt}(t,d_c) = \tilde{C}_{ntnt} \end{aligned} \tag{19}$$

where, in the case of undamaged elastic bricks, the stiffness components $\tilde{C}_{ijkl}$ are provided by the extension of the Cecchi and Tralli expressions (10) to the cracked state of the mortar joints. Accordingly viscous Young's modulus '$E_m(1+\phi_m(t))$' or equivalently the inverse creep function $J_m^{-1}(t)$ is simply substituted by $J_m^{-1}(t,d_c)$ which accounts for the crack density parameter.

Similarly to the undamaged elastic case, the proposed solution is expected to be an upper bound for the masonry stiffness. Recently, based on the works of Cecchi & Sab, Cecchi & Barbieri [13] and Cecchi & Tralli, Cecchi & Taliercio [12] have proposed a homogenized compliance for viscoelastic undamaged masonry with mortar joints assimilated to interfaces. In this paper we propose to extend also this model to microcracked masonry with finite dimensions of microcracked mortar joints. The

effective compliance of the damaged viscoelastic masonry reads then:

$$\begin{aligned}
\tilde{S}^R_{1111}(t,dc) &= \frac{S^b_{1111}\dfrac{e_v}{a+e_h}J'_v(t,dc) + 4S^b_{1111}\dfrac{e_h}{b+e_v}J'_h(t,dc) + 4\dfrac{e_v e_h}{(b+e_v)^2}J'_v(t,dc)J''_h(t,dc)}{4\dfrac{e_h}{b+e_v}J''_h(t,dc) + \dfrac{e_h}{a+e_h}J'_v(t,dc)} \\
\tilde{S}^R_{2222}(t,dc) &= S^b_{2222} + \frac{e_h}{a+e_h}J'_h(t,dc) \\
\tilde{S}^R_{1212}(t,dc) &= S^b_{1212} + \frac{e_h}{a+e_h}J''_h(t,d_c) + \frac{e_v}{b+e_v}J''_v(t,dc) - \frac{\dfrac{e_v^2}{(b+e_v)(a+e_h)}J''^2_v(t,dc)}{4\dfrac{e_h}{b+e_v}J'_h(t,dc) + \dfrac{e_v}{a+e_h}J''_v(t,dc)} \\
\tilde{S}^R_{1122}(t,dc) &= S^b_{1122}
\end{aligned} \tag{20}$$

The damaged masonry's effective moduli are then the following: $\tilde{E}_{11}(t,d_c) = \dfrac{1}{\tilde{S}^R_{1111}(t,d_c)}$, $\tilde{E}_{22}(t,d_c) = \dfrac{1}{\tilde{S}^R_{2222}(t,d_c)}$, $\tilde{\mu}_{12}(t,d_c) = \dfrac{1}{\tilde{S}^R_{1212}(t,d_c)}$, $\tilde{\nu}_{ij}(t,d_c) = -\tilde{E}_{ii}(t,d_c)\tilde{S}^R_{iijj}(t,d_c)$, where $(i,j) \in \{1,2\}$. These properties are explicit function of the crack density - damage parameter -, time and ratios $\dfrac{e_h}{a+e_h}$, $\dfrac{e_v}{b+e_v}$ instead of respectively $\dfrac{e_h}{a}$ and $\dfrac{e_v}{b}$. It is worth noting, that for the case of undamaged mortar interfaces, Cecchi & Taliercio have proven that this solution is more consistent with a numerically homogenized solution based on the finite elements method for ratios $E_b/E_m \geq 20$ when the mortar follows a Generalized Maxwell model. In the following, we assume that this condition ensuring the accuracy of the Cecchi & Taliercio's analytical model with the additional assumption of finite joints dimensions is also available for damaged mortars.

Hereafter mortar will follow typical Burgers and Modified Maxwell models. Moreover, the effective moduli of masonry proposed by Cecchi & Tralli and Cecchi & Taliercio will be extended to the damaged case of masonry with finite dimensions of joints without any recourse to numerical inversion of the Laplace Carson method. The yet proven accuracy of the Cecchi & Taliercio's analytical model for ratios $E_b/E_m \geq 20$ will be useful to assess the accuracy of the Cecchi & Tralli's extension model to damaged mortars.

3. Rheological models for undamaged mortar

The rate-dependent mechanical behaviour of mortar is often approximated by a linear viscoelastic model [17, 28]. For the sake of simplicity, only non-aging formulation will be considered in this work. The practical interest of this simple formulation is that it allows to transform a time-dependent boundary value problem into a linear elastic one using the well-known correspondence theorem based on the Laplace-Carson transform. Among the simplest formulations used to model the non-aging

linear viscoelastic mortar's behaviour, it is possible to quote the USBR, Ross, Feng, Burgers and Modified Maxwell models [17, 15] mainly based on connections in parallel and/or in series of Maxwell and Kelvin-Voigt parts. Each element (spring and dashpot) of the Maxwell (M) or Kelvin-Voigt (KV) model is characterized by an isotropic fourth-order tensor related to its elasticity or viscosity

$$\begin{aligned} C_K^e &= 3k_K^e J + 2\mu_K^e K, \qquad & C_K^v &= \eta_K^s J + \eta_K^d K, \\ C_M^e &= 3k_M^e J + 2\mu_M^e K, \qquad & C_M^v &= \eta_M^s J + \eta_M^d K \end{aligned} \tag{21}$$

where k_α and μ_α ($\alpha = K$ or M) denote the bulk and shear moduli. η_α^s and η_α^d represent respectively the bulk and shear viscosity. In the following, only rheological MM's model is presented.

Modified Maxwell model (MM). The constitutive law of the MM's model (see Figure (1)-j) is given by

$$S_M^v \sigma + S_M^e \dot{\sigma} = S_M^v C_R^e \varepsilon + (I + S_M^e C_R^e)\dot{\varepsilon} \tag{22}$$

where, for isotropic mortar material, the elastic and viscous compliances of the Maxwell part are given respectively by $S_M^e = \dfrac{1}{3k_M^e} J + \dfrac{1}{2\mu_M^e} K$ and $S_M^v = \dfrac{1}{\eta_M^s} J + \dfrac{1}{\eta_M^d} K$. The elastic stiffness of the spring reads $C_R^e = 3k_R^e J + 2\mu_R^e K$.

The Laplace-Carson transform applied to the behaviour law (22) leads to

$$(S_M^v + pS_M^e)\sigma^* = (S_M^v C_R^e + p(I + S_M^e C_R^e))\varepsilon^* \tag{23}$$

and allows the definition of the following symbolic Modified Maxwell elastic compliance

$$\mathbf{S}_{MM}^* = (S_M^v C_R^e + p(I + S_M^e C_R^e))^{-1}(S_M^v + pS_M^e) \tag{24}$$

Assuming the isotropy of the mortar behaviour, the symbolic compliance (24) reads

$$\mathbf{S}_{MM}^* = \frac{1}{3k_s^*} J + \frac{1}{2\mu_s^*} K \tag{25}$$

The associated apparent creep function is then given by

$$J_{MM}^* = \frac{1}{E_{MM}^*} = \frac{1}{9k_s^*} + \frac{1}{3\mu_s^*} = \frac{1}{9\left(k_R + \dfrac{pk_M\eta_M^s/3}{k_M + p\eta_M^s/3}\right)} + \frac{1}{3\left(\mu_R + \dfrac{p\mu_M\eta_M^d/2}{\mu_M + p\eta_M^d/2}\right)} \tag{26}$$

since

$$\frac{1}{k_s^*} = \frac{1}{\left(k_R + \dfrac{pk_M\eta_M^s/3}{k_M + p\eta_M^s/3}\right)}, \qquad \frac{1}{\mu_s^*} = \frac{1}{\left(\mu_R + \dfrac{p\mu_M\eta_M^d/2}{\mu_M + p\eta_M^d/2}\right)}. \tag{27}$$

The analytical direct inversion of (26) leads to the MM's real creep function

$$J_{MM}(t) = \frac{1}{9k_R} + \frac{1}{3\mu_R} - \frac{k_M}{9k_R(k_R+k_M)}e^{-t/\tau^s_{MM}} - \frac{\mu_M}{3\mu_R(\mu_R+\mu_M)}e^{-t/\tau^d_{MM}} \tag{28}$$

with the characteristic times $\tau^s_{MM} = \dfrac{\eta^s_M(k_R+k_M)}{3k_Rk_M}$ and $\tau^d_{MM} = \dfrac{\eta^d_M(\mu_R+\mu_M)}{2\mu_R\mu_M}$ for respectively the spherical and deviatoric parts of the MM's viscous behaviour.

4. Creep function of microcracked non-aging linear viscoelastic mortar

We consider a RVE Ω made up of non-aging linear viscoelastic material and a network of plane penny-shaped cracks. In contrast to 3D ellipsoidal crack model considered in the Eshelby-type approach, the mathematical penny-shaped crack is a 2D problem in nature which does not refer to an aspect ratio w. During the time period of loading, assuming that the displacement $u(z,t)$ prescribed on the boundary $\partial\Omega$ is given by $u(z,t) = \bar{\varepsilon}(t).z$ where the macroscopic strain $\bar{\varepsilon}(t)$ is the sum of the contribution of the elastic solid and of the fractures as follows

$$\bar{\varepsilon} = \frac{1}{V}\left(\int_{\Omega_s}\varepsilon dV + \sum_i\int_{C_i}[u]_i \otimes^s n_i dS\right) \tag{29}$$

where Ω_s is the domain of the undamaged matrix and $a \otimes^s b = \dfrac{a \otimes^t b + b \otimes^t a}{2}$ for the vectors a and b. C_i and n_i denote respectively the boundary of the crack i and the vector normal to its plane. For empty cracks, the overall stress reads $\Sigma =< \sigma >_\Omega = \dfrac{1}{V}\int_{\Omega_s}\sigma dV = \tilde{C} : \bar{\varepsilon}$ since the local stress in the voids is null.

4.1. Symbolic space: coupling between homogenization and Griffith's theory

The Laplace-Carson transform of the macroscopic strain (29) reads:

$$\bar{\varepsilon}^* = \frac{1}{V}\left(\int_{\Omega_s}\varepsilon^* dV + \sum_i\int_{C_i}[u]^*_i \otimes^s n_i dS\right)\bar{\varepsilon}^* = C^{*-1} : \Sigma^* + \frac{1}{V}\sum_i\int_{C_i}[u]^*_i \otimes^s n_i dS \tag{30}$$

In the framework of the stress-based dilute scheme [22], the displacement jump $[u]_i$ is linearly related to Σ. Indeed, the normal displacement jump (mode I) at the lips of a crack in an infinite matrix submitted to an isotropic asymptotic macroscopic stress $\mathbf{\Sigma}^* = \Sigma^*\,\mathbf{i}$ can be written:

$$[u_n]^* = \frac{4(1-\nu^*_s)}{\pi}\frac{\Sigma^*}{\mu^*_s}\sqrt{l^2-\rho^2}. \tag{31}$$

where l is the crack's radius and ρ is the position of a point M pertaining to the crack's plane. The tangential displacement jump (mode II) under an asymptotic shear stress $\mathbf{\Sigma}^* = \Sigma^* \mathbf{n} \otimes^s \mathbf{t}$ where t is parallel to the crack's plane reads:

$$[u_t]^* = \frac{4(1-\nu_s^*)}{\pi(2-\nu_s^*)} \frac{\Sigma^*}{\mu_s^*} \sqrt{l^2 - \rho^2}. \tag{32}$$

Effective dilute symbolic bulk moduli. Under an isotropic loading ($\Sigma^* = \Sigma : i$), the elementary contribution of a crack to the macroscopic strain is purely normal ($[u]^* = [u_n]^* n$) as shown in (31) and reads:

$$\int_{C_i} [u_n]_i^* \otimes^s n_i dS = \frac{8l^3}{3} \frac{\Sigma^*(1-\nu_s^*)}{\mu_s^*} n \otimes n \tag{33}$$

Assuming that all cracks have the same radius l, an integration over all orientations on the unit sphere yields the total crack contribution:

$$\frac{1}{V} \sum_i \int_{C_i} [u_n]^* \otimes^s n dS = \frac{8l^3}{3} \frac{\Sigma^*(1-\nu_s^*)}{\mu_s^*} \int_{|n|=1} n \otimes n \frac{dS}{4\pi} = \frac{8Nl^3}{9} \frac{\Sigma^*(1-\nu_s^*)}{\mu_s^*} i \tag{34}$$

where N denotes the number of cracks per unit volume. Combining (30) and (34) defines the effective state equation under isotropic loading:

$$\bar{\varepsilon}^* = C^{*-1} : (\Sigma^* : i) + \frac{8d_c}{9} \frac{\Sigma^*(1-\nu_s^*)}{\mu_s^*} i \tag{35}$$

for the damage parameter $d_c = N l^3$ [10, 23]. At last, since

$$trace(\bar{\varepsilon}^*) = \frac{\Sigma^*}{\tilde{k}_{DL}^*} = \left(\frac{1}{k_s^*} + \frac{8d_c}{3} \frac{(1-\nu_s^*)}{\mu_s^*} \right) \Sigma^* \tag{36}$$

then $\dfrac{1}{\tilde{k}_{DL}^*} = \dfrac{1}{k_s^*} + \dfrac{8d_c}{3} \dfrac{(1-\nu_s^*)}{\mu_s^*}$, or equivalently

$$\frac{1}{\tilde{k}_{DL}^*} = \frac{1 + d_c Q^*}{k_s^*} \quad \text{where} \quad Q^* = \frac{16}{9} \frac{(1-\nu_s^{*2})}{(1-2\nu_s^*)} \tag{37}$$

in which the symbolic Poisson's ratio of the undamaged matrix reads: $\nu_s^* = \dfrac{3k_s^* - 2\mu_s^*}{6k_s^* + 2\mu_s^*}$.

Effective dilute symbolic shear moduli. Under a deviatoric loading in which the macroscopic stress reads $\Sigma^* = \Sigma^*(e_1 \otimes e_1 - e_3 \otimes e_3)$, the elementary contribution of a crack to the macroscopic strain is derived from (31) and (32) according to its orientation. In the polar coordinates system (r, θ, Φ), the displacement jump is given by

$$[u]^* = \frac{\Sigma^*(1-\nu^*)}{\pi\mu^*} \left(X_r e_r + \frac{2}{2-\nu^*} (X_\theta e_\theta + X_\Phi e_\Phi) \right) \sqrt{a^2 - \rho^2} \tag{38}$$

if the normal vector n coincides with the radial unit vector e_r. Integration over all crack orientations on the unit sphere yields

$$\frac{1}{V}\sum_i \int_{C_i} [u]_i^* \otimes^s n_i dS = \frac{d_c M^*}{2\mu^*}\Sigma^* \quad \text{where} \quad M^* = \frac{32}{45}\frac{(1-\nu_s^*)(5-\nu_s^*)}{2-\nu_s^*} \tag{39}$$

Accordingly and due to (30), the apparent effective shear modulus reads

$$\frac{1}{\tilde{\mu}_{DL}^*} = \frac{1+d_c M^*}{2\mu_s^*} \tag{40}$$

4.2. Creep function: identification of existent rheological models at short and long times

Since the expressions (37) and (40) can not be satisfied rigorously, it was proposed in [36] to identify the best approximation of the effective behaviour in the class of Burgers' (Modified Maxwell's) model if the mortar in its undamaged state follows the Burgers' (Modified Maxwell's) model. The idea is to satisfy the series expansion of the dilute estimates of the bulk's (37) and shear (40) moduli to the first order at $p = 0$ and $p \to \infty$ such that

$$\lim_{t\to\infty} f(t) = \lim_{p\to 0} f^*(p) \quad \text{and} \quad \lim_{t\to 0} f(t) = \lim_{p\to\infty} f^*(p) \tag{41}$$

Hereafter, only the identification of the MM's creep parameters function will be detailed. Parameters related to the Burgers creep function at damaged state [37, 33] are reported in Appendix (A).

4.2.1. Expansions of the mortar's effective dilute apparent moduli

At the vicinity of $p = 0$, the expansions in series of $\frac{1}{k_s^*} = \frac{1}{k_R^s} + O(p)$ (see equation (27)-a) and $\frac{1}{\mu_s^*} = \frac{1}{\mu_R^s} + O(p)$ (equation (27)-b) provide the following approximations

$$\frac{1}{\tilde{k}_{DL}^*} = \frac{(1+d_c Q_0^0)}{k_R^s} + O(p), \qquad \frac{1}{\tilde{\mu}_{DL}^*} = \frac{(1+d_c M_0^0)}{\mu_R^s} + O(p) \tag{42}$$

where the coefficients Q_0^0, Q_0^1, M_0^0 and M_0^1 are given by

$$\begin{aligned} Q_0^0 &= \frac{4k_R^s(3k_R+4\mu_R)}{3\mu_R(3k_R+\mu_R)}, \quad Q_0^1 = \frac{2}{9}\frac{(2\eta_M^s\mu_R - 3k_R\eta_M^d)(9k_R^2+4\mu_R^2+6k_R\mu_R)}{\mu_R^2(3k_R+\mu_R)^2} \\ M_0^0 &= \frac{16}{45}\frac{(3k_R+4\mu_R)(9k_R+4\mu_R)}{(3k_R+\mu_R)(3k_R+2\mu_R)}, \quad M_0^1 = \frac{8}{45}\frac{(3k_R\eta_M^d - 2\eta_M^s\mu_R)(63k_R^2+60k_R\mu_R+16\mu_R^2)}{(3k_R+\mu_R)^2(3k_R+2\mu_R)^2}. \end{aligned} \tag{43}$$

On the other hand, at the vicinity of $p=\infty$, $\dfrac{1}{k_s^*}=\dfrac{1}{k_K^e+k_M^e}+\dfrac{3k_M^2}{(k_M^e+k_R^s)^2\eta_M^s\,p}+O(p^{-2})$ and $\dfrac{1}{\mu_s^*}=\dfrac{1}{\mu_K^e+\mu_M^e}+\dfrac{2\mu_M^2}{(\mu_M^e+\mu_R^s)^2\eta_M^d\,p}+O(p^{-2})$, accordingly

$$\begin{cases}\dfrac{1}{\tilde{k}_{DL}^*}=\dfrac{1+d_cQ_0^\infty}{k_M^e+k_R^s}+\dfrac{1}{p}\dfrac{(3k_M^2(1+d_cQ_0^\infty)+d_c(k_M^e+k_R^s)Q_1^\infty\eta_M^s)}{\eta_M^s(k_M+k_R^s)^2}+O(1/p^2)\\ \dfrac{1}{\tilde{\mu}_{DL}^*}=\dfrac{1+d_cM_0^\infty}{\mu_M^e+\mu_R^s}+\dfrac{1}{p}\dfrac{\left(2\mu_M^2(1+d_cM_0^\infty)+d_c(\mu_M^e+\mu_R^s)M_1^\infty\eta_M^d\right)}{\eta_M^d(\mu_M+\mu_R^s)^2}+O(1/p^2)\end{cases}\tag{44}$$

where the coefficients Q_∞^0, Q_∞^{-1} and M_∞^0 are given by

$$\begin{aligned}Q_\infty^0&=\frac{4}{3}(k_M+k_R)(\frac{1}{\mu_M+\mu_R}+\frac{3}{3(k_M+k_R)+(\mu_M+\mu_R)}),\\ M_\infty^0&=\frac{16}{45}\left(8-\frac{9(k_M+k_R)}{3(k_M+k_R)+(\mu_M+\mu_R)}-\frac{6(k_M+k_R)}{3(k_M+k_R)+2(\mu_M+\mu_R)}\right)\end{aligned}\tag{45}$$

4.2.2. Identification of an existent rheological model for the cracked mortar's creep function

The dilute symbolic bulk's (37) and shear's (40) moduli of a non-aging linear viscoelastic (n.a.l.v.) microcracked mortar following the MM's model can be approached by expressions similar respectively to (27)-a and (27)-b available for a mortar with a matrix following the MM's rheological model

$$k_{MM}^*=k_R(d_c)+\frac{pk_M(d_c)\eta_M^s(d_c)/3}{k_M(d_c)+p\eta_M^s(d_c)/3},\quad \mu_{MM}^*=\mu_R(d_c)+\frac{p\mu_M(d_c)\eta_M^d(d_c)/2}{\mu_M(d_c)+p\eta_M^d(d_c)/2}\tag{46}$$

The series expansion of the dilute symbolic estimate of the bulk's modulus $\dfrac{1}{\tilde{k}_{DL}^*}$ (respectively shear modulus $\dfrac{1}{\tilde{\mu}_{DL}^*}$) and its approximation $\dfrac{1}{\tilde{k}_{MM}^*}$ (respectively $\dfrac{1}{\tilde{\mu}_{MM}^*}$) at the vicinity of 0

$$\frac{1}{\tilde{k}_{MM}^*}=\frac{1}{k_R(d_c)}-p\frac{\eta_M^s(d_c)}{3k_R^2(d_c)}+O(p^2),\quad \frac{1}{\tilde{\mu}_{MM}^*}=\frac{1}{\mu_R(d_c)}-p\frac{\eta_M^d(d_c)}{2\mu_R^2(d_c)}+O(p^2)\tag{47}$$

and ∞

$$\begin{cases}\dfrac{1}{\tilde{k}_{MM}^*}=\dfrac{1}{k_R(d_c)+k_M(d_c)}+\dfrac{1}{p}\dfrac{3k_M^2(d_c)}{\eta_M^s(d_c)(k_M(d_c)+k_R(d_c))^2}+O(\dfrac{1}{p^2})\\ \dfrac{1}{\tilde{\mu}_{MM}^*}=\dfrac{1}{\mu_R(d_c)+\mu_M(d_c)}+\dfrac{1}{p}\dfrac{2\mu_M^2(d_c)}{\eta_M^d(d_c)(\mu_M(d_c)+\mu_R(d_c))^2}+O(\dfrac{1}{p^2})\end{cases}\tag{48}$$

added to the equalities $\dfrac{1}{k_{DL}^*}\approx\dfrac{1}{k_{MM}^*}$ and $\dfrac{1}{\mu_{DL}^*}\approx\dfrac{1}{\mu_{MM}^*}$ allow the identification of the following six MM's parameters

$$\begin{aligned}k_R(d_c)&=\frac{k_R}{1+d_cQ_0^0}, & \mu_R(d_c)&=\frac{\mu_R}{1+d_cM_0^0}\\ k_M^e(d_c)&=\frac{k_M+k_R}{1+d_cQ_0^\infty}-\frac{k_R}{1+d_cQ_0^0}, & \eta_M^s(d_c)&=\frac{(\eta_M^s+d_c(\eta_M^sQ_0^0-3k_R^eQ_0^1))}{(1+d_cQ_0^0)^2}\\ \mu_M(d_c)&=\frac{\mu_M+\mu_R}{1+d_cM_0^\infty}-\frac{\mu_R}{1+d_cM_0^0}, & \eta_M^d(d_c)&=\frac{\eta_M^d+d_c(\eta_M^dM_0^0-2\mu_RM_0^1)}{(1+d_cM_0^0)^2}\end{aligned}\tag{49}$$

The characteristic times of the spherical and deviatoric parts of the Modified Maxwell model followed by the microcracked viscoelastic mortar are respectively

$$\tau^s_{MM}(d_c) = \frac{\eta^s_M(d_c)(k_R(d_c)+k_M(d_c))}{3k_R(d_c)k_M(d_c)}, \quad \tau^d_{MM} = \frac{\eta^d_M(d_c)(\mu_R(d_c)+\mu_M(d_c))}{2\mu_R(d_c)\mu_M(d_c)} \tag{50}$$

At last, the approximate creep function of a microcracked mortar which matrix follows the MM's model reads

$$J^{app}_{MM}(t,dc) = \frac{1}{9k_R(d_c)}\left(1-\frac{k_M(d_c)}{(k_R(d_c)+k_M(d_c))}e^{-t/\tau^s_{MM}(d_c)}\right)+\frac{1}{3\mu_R(d_c)}\left(1-\frac{\mu_M(d_c)}{(\mu_R(d_c)+\mu_M(d_c))}e^{-t/\tau^d_{MM}(d_c)}\right) \tag{51}$$

5. Application for a 2D masonry with microcracked viscoelastic hybrid mortar

To assess the reliability of the Cecchi & Tralli extension model presented in this paper, it is proposed, in a first step (s_1) (see Figure (1)), to implement the creep functions (53) and (51) and to study the effects of the crack density d_c, time t and geometrical parameter $\beta = E_b/E_m$ on the trends of the creep of the mortar. As mentioned previously (see section (2.2.2)), the estimates of the Cecchi & Taliercio extension model are useful as reference solution since the accuracy of this model at undamaged case has been yet proven in [12] by comparison with more accurate finite element solution. Based on this result, only elastic bricks with Young's moduli $E_b \geq 20E_m(t_0)$ (here the initial time t_0 is set equal to 0) will be considered in the following. For these evaluations, the adopted mortar's data are given in table-1. The properties of the undamaged bricks are the following: $\nu_b = \nu_m$ and $E_b = 100E_m(t_0)$ where for this hybrid mortar $E_m(t_0) = J^{-1}_{MM}(t_0,\ 0) = 6150$ MPa for the MM's model and $J^{-1}_{Bu}(t_0,\ 0) = 4038$ MPa for the Burgers' one. Recall here that $J^{-1}_{MM}(0,\ 0) = E_R + E_M$ and $J^{-1}_{Bu}(0,\ 0) = E_M$. Bricks are of dimensions 250x55 mm^2 and mortar's joints thicknesses are $e_h = e_v = 10\,mm$. Effective masonry's moduli for cases $E_b = 40E_m(t_0)$ and $20E_m(t_0)$ allowing to study the effect of the parameter β are reported in Appendix (B). Note that the characteristic times

E_M (MPa)	τ_M (s)	E_R (MPa)	τ_R (s)	ν_m
4038	46490	2112	90866	0.22

Table 1: Elastic and viscous moduli of hybrid mortar [28]

for the spherical and deviatoric hybrid mortar's behaviour are assumed to be equal $\tau^s = \tau^d = \tau$ for the MM's and Burgers' models. The Young's modulus E_R and Poisson's ratio ν_R coincide respectively with E_K and ν_K, properties of the Kelvin-Voigt's spring.

For damaged state, to validate the step (s_1), comparisons with results provided by Nguyen et al. [36] for concrete material following the typical Burgers model were carried out. Moreover the evolutions of the MM's model parameters identified in section (4.2.2) versus the crack density d_c depicted in Figure (13) in Appendix (7) validate this identification step since these parameters decrease with the increase of the damage parameter. Similar validation procedure was carried out for the Burgers parameters but is not reported in this paper for the sake of brevity.

In this work, the validity of the step (s_2) was ensured by comparisons with Cecchi & Sab [14] effective stiffnesses available for elastic undamaged masonry either with plane strain or plane stress hypothesis (see table-2 in [14]). When accounting for the creep effects, this model was validated by making comparisons with Cecchi & Tralli results available for periodic masonry with undamaged ($d_c = 0$) mortar following the USBR rheology model (see Figure (7) in [15]). Note that in this paper, the implemented effective stiffness components $\tilde{A}_{2222}$ and $\tilde{A}_{1212}$ are similar to those proposed by Cecchi & Sab [14] (see equation (10)) but accounting for creep and finite dimensions of mortar joints.

5.1. Evolutions of the normalized inverse dilute creep functions $J_{DL}^{MM^{-1}}$ and $J_{DL}^{Bu^{-1}}$ of the mortar joints

Figure (3) and (4) illustrate the evolutions of normalized inverse dilute creep functions of respectively the MM's and Burgers' models with respect to the damage parameter d_c and the time t. When the

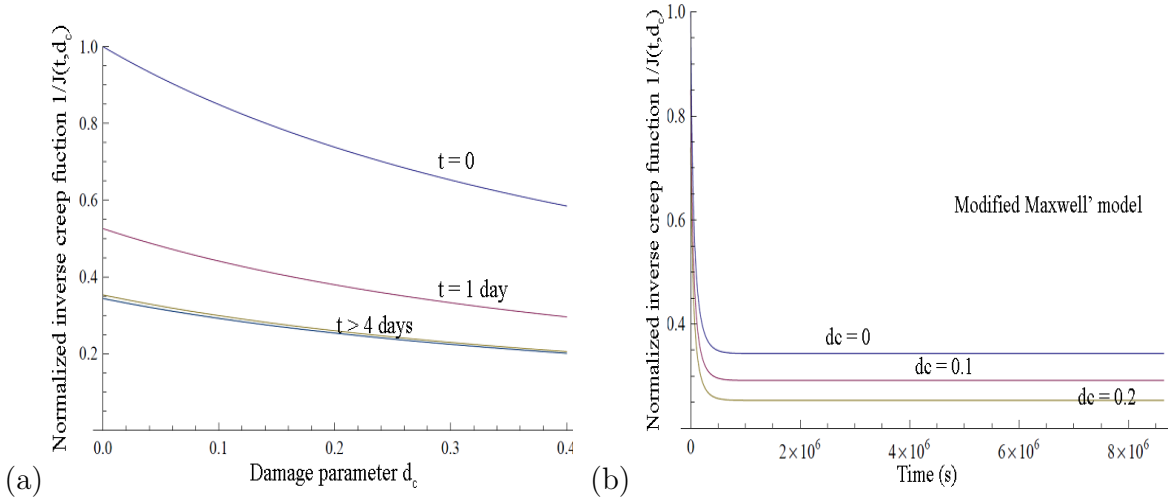

Figure 3: *Mortar following the MM's model: Variation of $J_{MM}^{-1}(t, d_c)/J_{MM}^{-1}(0, 0)$ versus time (b) for undamaged mortar ($d_c = 0$) and microcracked mortars ($d_c = 0.1$, $d_c = 0.2$) and (a) versus the damage parameter d_c at different times $t = 0$, 1 day and $t \geq 5$ days.*

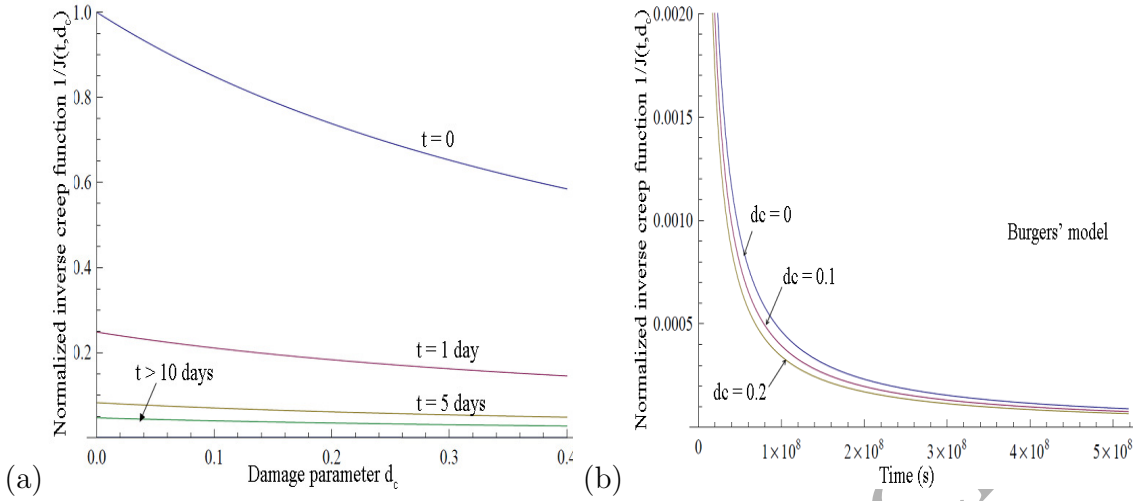

Figure 4: *Mortar following the Burgers's model: Variation of* $J_{Bu}^{-1}(t,d_c)/J_{Bu}^{-1}(0,0)$ *versus time (b) for undamaged mortar* ($d_c = 0$) *and microcracked mortars* ($d_c = 0.1$, $d_c = 0.2$) *and (a) versus the damage parameter* d_c *at different times* $t = 0$, 1, 5 *days and* $t \geq 10$ *days.*

damage parameter d_c increases, Figure(3)-a (respectively (4)-a) shows that the normalized inverse creep function $J^{-1}(t,d_c)/J^{-1}(0,0)$ does not evolve beyond $t \geq 5$ days for the MM's (respectively, 10 days for the Burgers') model. Moreover, unlike the Burgers' model, the MM's one predicts a slower decrease of the normalized creep function versus the damage parameter d_c. Indeed, for the considered mortar with properties gathered by means of short term compressive tests on masonry wallets [28], this function vanishes for times exceeding 10 days according to this version of the Burgers model whereas the MM's estimates tend towards non-zero asymptotic limits for $t \geq 5$ days.

For a given crack density parameter $d_c = 0$, 0.1 or 0.2, Figure (3)-b demonstrates that the MM's model yields to a constant function $J^{-1}(t,d_c)/J^{-1}(0,0)$ with variation of the time beyond $t = 10^6$(s) (i.e. almost 11 days). As expected, the increase of d_c decreases the level of the asymptotic limits reached by this function. The difference between the MM's curves for different d_c is not negligible (around 15%) unlike that observed for the Burgers curves which are very close especially at short and long terms. Figure (4)-b shows again that the Burgers model leads to vanishing inverse creep functions for $t \geq 3\,10^8$ (s) i.e. 1157 days for every crack density value $d_c \geq 0$.

Recall here that this version of the Burgers model is different from the modified or adapted ones proposed in [34, 46, 47]. Parameters of these modified Burgers models - generally up to 15 - need experimental investigations to be identified so as experimental creep curves coincide with modified Burgers predictions.

5.2. Effective behaviour of periodic microcracked viscoelastic masonry cell

5.2.1. Constant crack density d_c

In this part, it is assumed that crack does not propagate following the Nguyen et al. [37, 39] researches. Tables (2) and (3) provide the effective properties of a periodic masonry cell with hybrid viscoelastic mortar at its undamaged and microcracked states with quasi-rigid ($E_b = 100E_m(t_0)$) bricks. Tables (4) to (7) reported in Appendix (7) give the effective properties of a periodic viscoelastic masonry cell with respectively $E_b = 20E_m$ and $E_b = 40E_m$. For the considered hybrid mortar, these tables demonstrate that the effective properties of a masonry cell with a microcracked mortar following the Burgers model vanish of about 99% by reference to the undamaged state for any range of the stiffnesses ratio $\beta = \dfrac{E_b}{E_m} \in [20, 100]$. The evaluation of the absolute error E_r between masonry cell's effective properties at undamaged and damaged ($t = 1000$ days, $d_c = 0.1$) states for the MM's model shows that this error increases with the increase of the ratio β to reach a maximum of about 71% which is an asymptotic limit for E_r attained in the case of quasi-rigid bricks ($E_b = 100E_m$). This result demonstrates that the MM's model allows the masonry to preserve a certain resistance for $\beta \geq 20$ unlike this version of the Burgers model for which the masonry seems to fail. Figures (5) and (6) depict the evolutions of the effective properties of the periodic

Mortar: rheological model	t (days)	d_c	$\tilde{E}_{tt}$ (MPa)	$\tilde{E}_{nn}$ (MPa)	$\tilde{\nu}_{tn}$	$\tilde{\nu}_{nt}$	$\tilde{\mu}_{tn}$ (MPa)
Burgers	0	0	111223.	11792.8	0.037	0.004	8087.07
	25	0	3082.32	142.66	0.002	0	202.6
	25	0.1	2620.62	120.77	0.0016	0	172.17
	100	0	810.81	36.74	0	0	53.18
	100	0.1	688.77	31.17	0	0	45.17
	1000	0	82.37	3.70	0	0	5.4
	1000	0.1	69.95	3.15	0	0	4.58
Modified Maxwell	0	0	169277	39314.9	0.060	0.0140	14432.7
	≥ 100	0	70955.6	14095.1	0.025	0.005	5150.
	≥ 100	0.1	61324.4	12011.6	0.022	0.004	4387.1
Absolute error E_r (%)			63.7	69.4	63.5	71.4	69.6

Table 2: Cecchi & Tralli's extension model: effective properties of a periodic masonry cell with quasi-rigid bricks ($E_b = 100E_m$) and hybrid viscoelastic mortar [28]

masonry cell as functions of the crack density parameter d_c and time t. As expected, the normal-

Mortar: rheological model	t (days)	dc	$\tilde{E}_{tt}$ (MPa)	$\tilde{E}_{nn}$ (MPa)	$\tilde{\nu}_{tn}$	$\tilde{\nu}_{nt}$	$\tilde{\mu}_{tn}$ (MPa)
Modified Maxwell	0	0	164964.	37535.2	0.060	0.0134	14400.6
	≥ 100	0	68761.2	13428.3	0.0245	0.0050	5138.13
	≥ 100	0.1	59395.3	11441.3	0.0212	0.004	4376.9
Maxi. absolute error $E_r^{'}$ (%)			3.24	4.98	3.3	5	0.023

Table 3: Cecchi & Taliercio's extension model: effective properties of a periodic masonry cell with quasi-rigid bricks ($E_b = 100E_m$) and hybrid viscoelastic mortar [28]

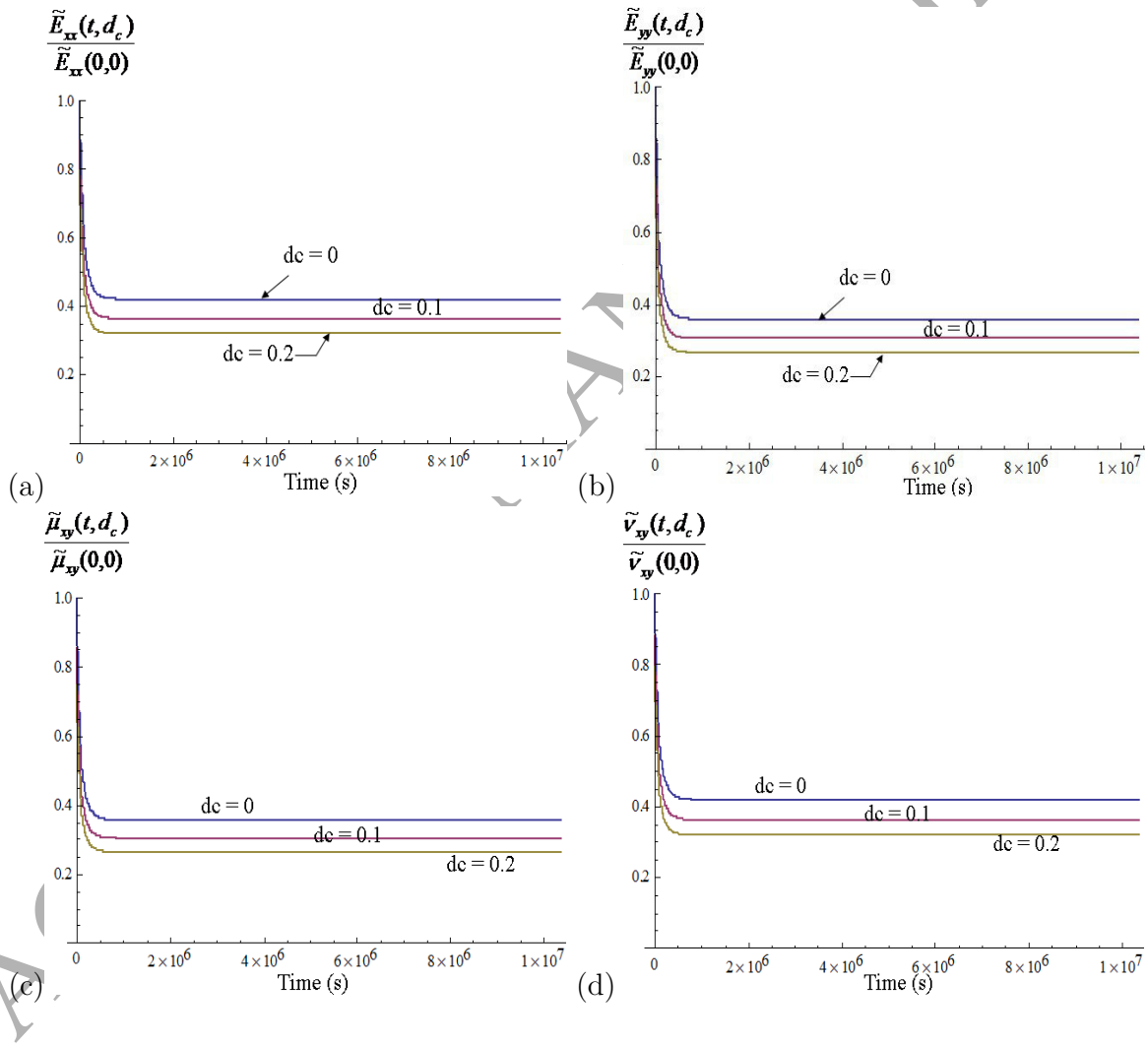

Figure 5: *MM's model: Evolutions of the effective properties of the periodic masonry cell as function of time for different crack density parameters* $d_c = 0,\ 0.1$ *and* 0.2

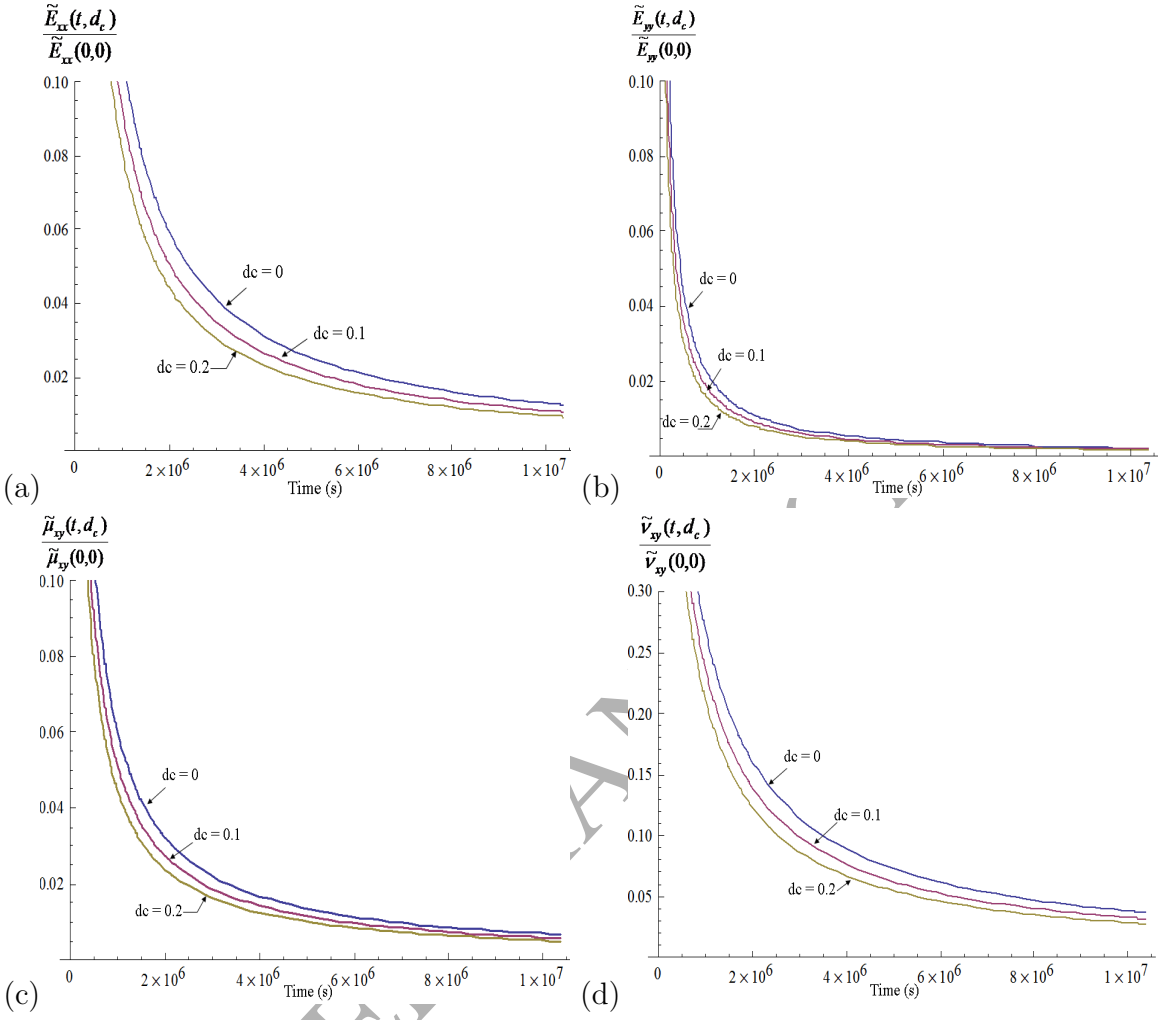

Figure 6: *Burgers' model: Evolutions of the effective properties of the periodic masonry cell as function of the time for different crack density parameters* $d_c = 0,\ 0.1$ *and* 0.2

ized effective moduli $\tilde{E}_{xx}(t,d_c)/\tilde{E}_{xx}(0,0)$, $\tilde{E}_{yy}(t,d_c)/\tilde{E}_{yy}(0,0)$, $\tilde{\mu}_{xy}(t,d_c)/\tilde{\mu}_{xy}(0,0)$ and Poisson's ratio $\tilde{\nu}_{xy}(t,d_c)/\tilde{\nu}_{xy}(0,0)$ decrease with the two parameters: t and d_c for both models MM and Burgers. For the considered mortar, similarly to the evolutions of the normalized inverse creep functions (see figures (3)), the evolutions of the periodic unit cell's effective properties with a mortar following the MM's rheological model decrease at the short time to reach a non-zero asymptotic limit at the medium and long terms unlike the predictions of the Burgers' model which vanish at short and long term for any value of $d_c \geq 0$. It is worth noting that time or duration highly softens the MM's effective properties of masonry (even without damage). For $E_b = 100E_m$, this can reach 65% for $\tilde{E}_{yy}$ and 55% for the $\tilde{E}_{xx}$ moduli (see Figure (5)) from the undamaged state after at least 100 days (see

Table-3). The crack density d_c accelerates this softening with an additional reduction of moduli of about 10% ($E_b = 20E_m$) and 13% ($E_b = 100E_m$) for $\tilde{E}_{tt}$. These results are consistent with those provided by Choi et al. [17]. Indeed, unlike the typical Maxwell model, the additional spring in this model's chain provides resistance after full relaxation which makes the long-term creep rate decrease continuously to better represent the realistic long-term behaviour of masonry. Moreover, it has been proven in [17] and confirmed by Shrive et al. [43] that the basic Burgers model only gives good results for the first few days (up to 100 days) and then exaggerates the creep strain. Similarly to the USBR model, the Burgers model represents continuously increasing creep deformation unlike the Ross, Feng and Modified Maxwell models which predict finite creep deformation at $t = \infty$. Indeed, for the MM model, the asymptotic infinite limit is $J_{MM}(t \to \infty, d_c) = \dfrac{1}{E_R(d_c)}$ for every crack density d_c (see equation (51)). Moreover, it has been shown that the Burgers model [17] exhibits a serious convergence problem when identifying the creep parameters of a number of testd experimental specimens. Accordingly, it has been concluded [17] that in most cases the MM's model can more accurately predict masonry creep compared with the Feng, Ross, USBR and even basic Burgers rheological models since when the MM's model, USBR and Ross models were applied to test data reported by Brooks and Bingel [9] and Shrive et al. [43], it provided the lowest prediction errors.
Note that disadvantages presented by creep predictions provided by the basic Burgers model for masonry - but not for concrete materials - have motivated some researchers to insert in this model a 'frictional' (or Bingham) element between the spring and the dashpot of the Maxwell element in order to prevent the activation of secondary creep at low stresses. Moreover they have added (static and viscous) damage parameters respectively in first and second Maxwell's components as proposed by Papa & Taliercio [34]. Other authors simply added viscous damage parameter as done by Verstrynge et al. For this damage variable (D_v), often evolution laws for brittle materials are used, such as for rock salt [16]. The main disadvantage of the modified Burgers models is their practical applicability since they involve significant number of parameters - up to 15 parameters for the global version - which need to be estimated according to experimental data. Moreover, they require a postulation or experimental investigation of the damage variables evolution laws. Although these disadvantages, modified Burgers models are more accurate and able to reproduce creep behaviour of masonry structures compared to the basic version of this model. Note that by analogy to the simple modified Burgers version (without the Bingham element) proposed by Verstrynge et al., it will be interesting to postulate a damage evolution law (similar to equation (5) in [46, 47]) - function of stress and time - and a damage rate formulation (as equation (6) [46, 47]) - function of stress - so as there is correlation between this version of the Burgers model and experimental creep tests provided in [34, 46, 47].

At last, as shown in tables (3), (6) and (8), for undamaged and damaged states, Cecchi & Taliercio's extension effective estimates are close to the Cecchi & Tralli's extension ones when the mortar behaves following the MM's model. The absolute error $E_r^{'}$ between the two models estimates increases with time and damage to reach a maximum of 5%. Recall that the MM's model leads to finite asymptotic limits for global moduli of damaged masonry (see Figures (5)). It is worth noting that the Cecchi & Taliercio estimates are softer than the Cecchi & Tralli ones for undamaged and damaged masonry's states. Accordingly, the Cecchi & Taliercio extension model seems to be more accurate than the Cecchi & Tralli's extension one. In this context, recall that the Cecchi & Tralli's estimate is expected to be upper bound for the exact overall solution [15].

5.2.2. Time-dependent crack density d_c

In this part, for the sake of simplicity, it is assumed that the crack density d_c is set equal to zero at the initial time $t_0 = 0$ and evolves linearly with time t as follows

$$d_c = \dot{d}_c\, t \tag{52}$$

where, here, the rate of the crack density $\dot{d}_c$ is assumed to be a positive constant lower than 0.002/day (i.e. if $t = 100$ days, then d_c reaches a maximum of 0.2). Indeed, beyond this limit, the dilute estimate will not be appropriate. Of course, as well known, the increase of the damage rate reduces the stiffness of the masonry cell. Table−4 provides time evolution of the effective moduli of a damaged masonry

Rheological model	t (days)	dc	$\tilde{E}_{tt}$ (MPa)	$\tilde{E}_{nn}$ (MPa)	$\tilde{\nu}_{tn}$	$\tilde{\nu}_{nt}$	$\tilde{\mu}_{tn}$ (MPa)
Modified Maxwell	0	0	164964.	37535.2	0.060	0.013	14400.6
	1	$1.5\,10^{-4}$	99349.4	20317.3	0.035	0.007	7780.04
	5	$7\,10^{-4}$	70366.6	13774.4	0.025	0.0049	5270.76
	40	$6\,10^{-3}$	68119	13290.3	0.024	0.0047	5085.25
	100	$1.5\,10^{-2}$	67177.8	13088.5	0.024	0.0047	5007.94
	500	$7.4\,10^{-2}$	61512.	11885.7	0.022	0.00425	4547.1
	1000	0.15	55645.6	10661.	0.02	0.004	4078.01
	1200	0.2	52163.2	9943.73	0.018	0.003	3803.36

Table 4: Exension of the Cecchi & Taliercio's model: effective properties of a periodic masonry cell with elastic bricks ($E_b = 100E_m$) and hybrid viscoelastic mortar accounting for time-dependent d_c with a constant rate $\dot{d}_c = 1.5\text{x}10^{-4}$/day.

cell when considering a linear time-dependent crack density (52) with $\dot{d}_c = 1.5\text{x}10^{-4}$/day. It can

be remarked that the effective moduli decrease quickly for $t \geq 5$ days. Beyond this limit, these moduli decrease slightly with time even if d_c increases. As proven previously, this table shows that effective properties of damaged masonry following the MM's model do not vanish for $d_c \leq 0.2$. For the considered mortar (see Table-1), similar evaluation of the effective properties of damaged masonry with a linear time-dependent crack density were carried out for the proposed extension to the Burgers model. This result showing vanishing effective moduli within about 20 days is not reported here for brevity. Owing to results depicted on Table$-$13, similar trends are obtained for mortar with long-term characteristic times (see Table-11 depicting elastic and viscous properties of tested specimens from the Pavia Tower [35]) but with effective properties tending towards 0 within higher duration (beyond 500 days). These trends change (see Table-14) when considering mortar with too high ($\tau_M \geq 10^7(s)$) values of the Maxwell's relaxation time τ_M (see Table-12) as it is the case of hybrid mortar with long-term characteristic times [47]. Indeed, in this case, the masonry's Burgers predictions, even though lower than MM's overall estimates, do not vanish after 1200 days with a crack density $d_c = 0.2$ (see Table-14). This demonstrates the relevance of the proposed Burgers model for the prediction of the long-term creep with very high values of the Maxwell's relaxation time $\tau_M \geq 10^8$ (s). Tables-15 and -16 related to mortars with long-term characteristic times with properties of respectively hybrid mortar [47] or similar to tested specimens from the Pavia Tower [35] confirm trends previously mentioned for the MM's model when dealing with mortar's properties gathered by means of short term compressive tests on masonry wallets [28]. The trends of the MM's model are then independent from the values of the Maxwell's relaxation time, short or long-term gathered properties of the mortar. At last, it is worth noting that similar stress and time dependent evolution law and damage rate to those proposed in [34, 46, 47] should be considered similarly in a future work.

6. Computation of the proposed model to the case of a compressed masonry panel

In this part, only the Cecchi & Taliercio extension estimates will be considered. In order to evaluate the relevance of the proposed extension model, we treat the case of a masonry panel of dimensions $L = 1560\, mm$ (length) and $H = 1040\, mm$ (height) studied in [15] subjected to boundary conditions BC$-$1 with three distributed loads at the top and two lateral edges (see Figure (7)-a) or BC$-$2 with an additional concentrated load F applied on the top as shown on Figure (7)-b. Bricks are assumed to be elastic or quasi-rigid. The mortar inside the joints is assumed to be microcracked with a matrix which obeys to linear viscoelastic behaviour following the Modified Maxwell's model. As the arrangement of the bricks is regular, the effective behaviour of the panel is assumed to be

well estimated by that of a periodic cell (see Figure 1-a). The panel can then be modeled as a homogeneous material which properties coincide with those of the equivalent material MHE-2 (see Figure (7)-c). The mortar's data used to compute this problem are provided in Table-1.

To validate this computation, it was checked that, under boundary condition BC−1, stress field

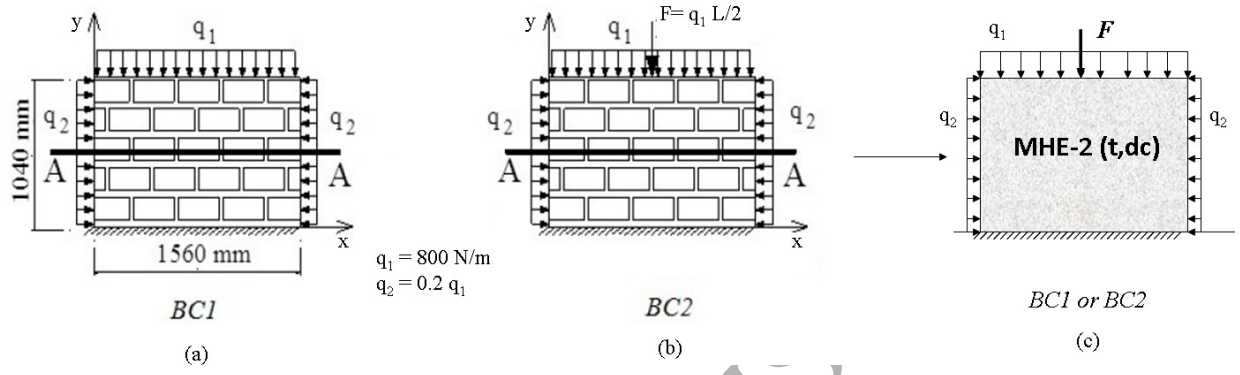

Figure 7: Equivalent problem (c) for the masonry panel submitted to boundary conditions BC−1 (a) or BC−2 (b).

σ_{yy} is 'almost' constant and each component of the stress field coincides for different times $t = 0$ and $t = 1000$ days. Recall that only local fields results derived from the MM's model are reported. Local mechanical estimates related to the Burgers model are commented but not reported here for concision purpose.

Qualitatively, under BC-1 and BC-2, distribution of the stress field σ_{yy} is symmetric (Figures (8)-b and (9)-b) by reference to the axis of symmetry of the panel $x = L/2$ unlike that of the stress σ_{xy} which is anti-symmetric (Figures (8)-a and (9)-a). Similar qualitative aspects are observed for snapshots of the strains ε_{yy} (symmetric, see (Figure (11)-b)) and ε_{xy} (anti-symmetric owing to Figure (11)-a). In this context, note that snapshot of the strain field ε_{yy} (ε_{xy}) induced in the wall by boundary conditions BC-1 is not illustrated here since qualitatively it presents similar trend to the σ_{yy} (σ_{xy}) stress map. Strain and stress fields show similar localization areas in both left and right higher corners of the wall (at the vicinity of the application's point of the concentrated load F) under conditions BC-1 (BC-2).

Quantitatively, similarly to boundary conditions BC-1, stress components are almost coincident under BC-2 for $t = 0$ and $t = 1000$ days independently of the damage state: $d_c = 0$ or $d_c = 0.15$. This quantitative aspect is confirmed by Figures (10) showing the evolutions of stress components along the x axis located at the middle height of the wall ($x = H/2$). On the other hand, the absolute values of the strain fields components increase with the increase of damage (Figures (12)). Moreover, under BC-1, strain values are lower than those attained under BC-2. Indeed, for a same damaged state $d_c = 0.15$, ratios between maximum absolute values of ε_{yy} reached under BC-2 and BC-1 at time

$t = 1000$ days is about 8. This ratio is around 2 for the strain ε_{xy}. Even lower than ε_{yy}, the strain ε_{xy} is more sensitive to the boundary condition BC-2. Quantitatively, for the considered mortar with sort-term gathered data, while stresses do not change throughout the wall between the two states ($t = 0$, $d_c = 0$) and ($t = 1000$ days, $d_c = 0.15$) for the MM's model, this field is amplified according to this version of the Burgers model under the boundary conditions BC$-$2. At last, under these boundary conditions, it is observed that the MM's model predicts small strains unlike those provided by this version of the Burgers model. For the later, there are great differences between the magnitudes of strain fields at undamaged ($t = 0$, $d_c = 0$) and damaged ($t = 100$ days, $d_c = 0.1$) states. Such results motivate to avoid modeling traditional mortars with short-term gathered properties using the Burgers model since it leads to vanishing masonry's stiffnesses and large strains increasing thus the risk of failure. These trends for the Burgers model are not valid if the Maxwell's relaxation time of the mortar is too high ($\tau_M \geq 10^7(s)$) as it is the case f hybrid mortar with long-term characteristic times (Table-12). In the later case, the Burgers model is expected to provide local fields predictions similar to the MM's estimates. The boundary conditions BC$-$1 are preferable to BC$-$2 since the later increases the stress and strain levels throughout the wall. Owing to Figures (8) and (9), at $t = 1000$ days, while failure occurs in the wall's area located around the application's point of the concentrated load F under BC-2, there is no failure in the wall submitted to conditions BC-1.

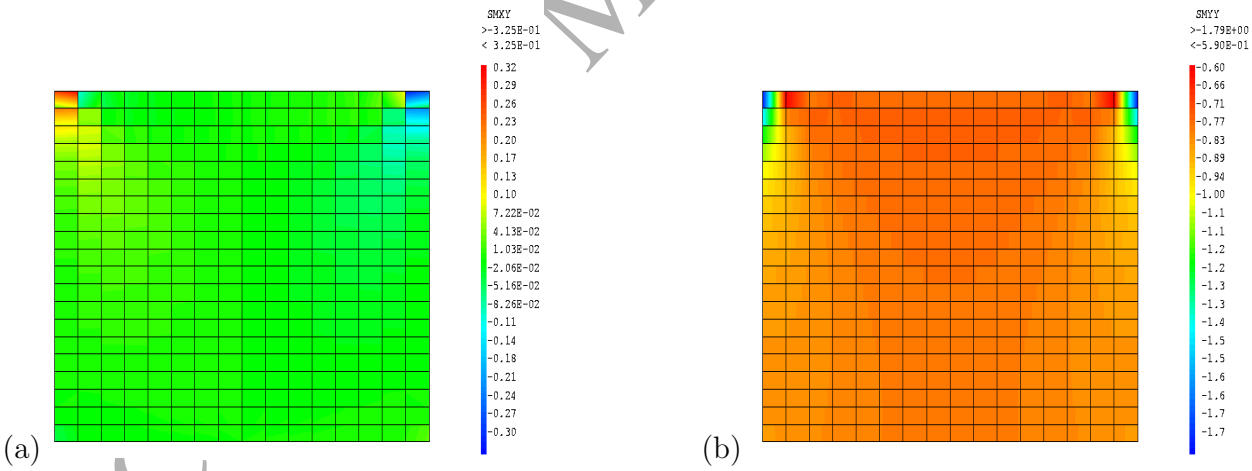

(a) (b)

Figure 8: *BC$-$1 boundary conditions: MM's model predictions of σ_{xy} (a) and σ_{yy} (b) maps for $d_c = 0.15$ at $t = 1000$ days. Here crack density $d_c = \dot{d}_c t$ where $\dot{d}_c = 1.5\,10^{-4}/day$.*

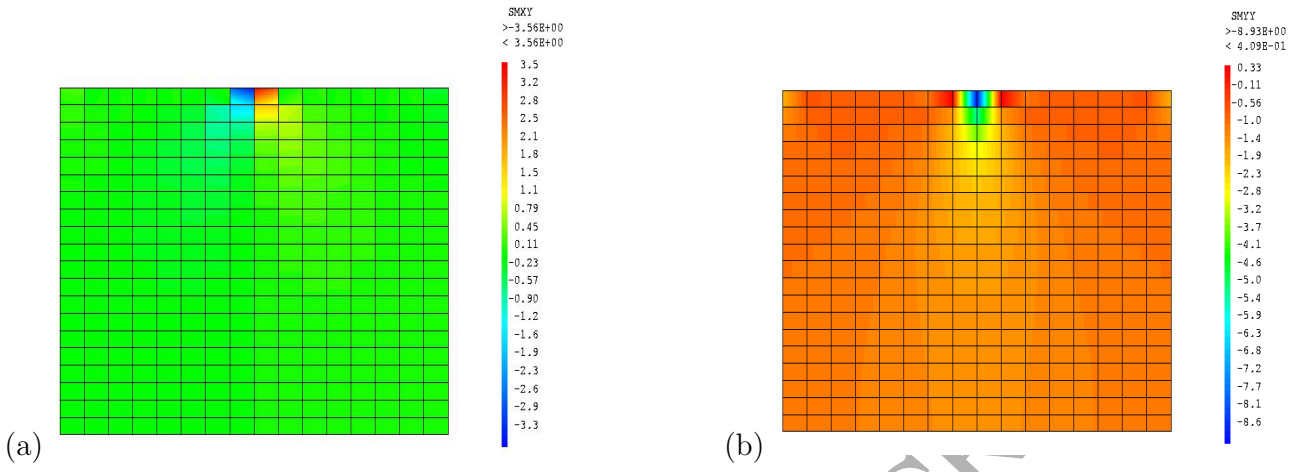

(a) (b)

Figure 9: *BC−2 boundary conditions: MM's model predictions for the maps of stresses* σ_{xy} *(a) and* σ_{yy} *(b) for* $d_c = 0.15$ *at* $t = 1000$ *days. Here crack density* $d_c = \dot{d}_c t$ *where* $\dot{d}_c = 1.5\,10^{-4}/day$.

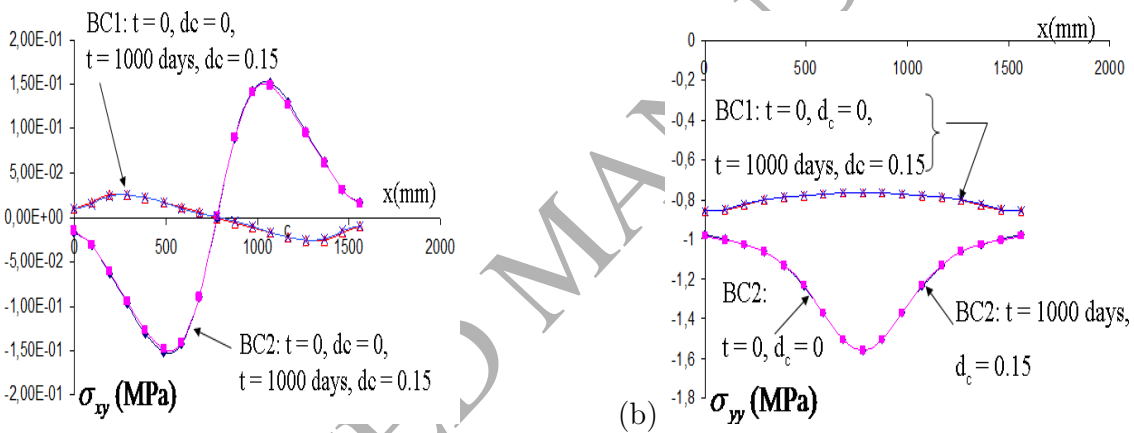

(a) (b)

Figure 10: *Boundary condition BC−1 or BC−2: trends in* σ_{xy} *(a) and* σ_{yy} *(b) at the panel section A-A for the Modified Maxwell's model at time* $t = 0$ *with* $d_c = 0$ *and* $t = 1000$ *days with* $d_c = 0.15$. *Here crack density* $d_c = \dot{d}_c t$ *where* $\dot{d}_c = 1.5\,10^{-4}/day$.

7. Conclusions and perspectives

In this paper extensions of the Cecchi & Tralli [15] and the Cecchi & Taliercio [12] models were proposed for microcracked non-aging viscoelastic masonry using the MM's and basic Burgers models. These extensions are based in a first step on the coupling between the Griffith's theory and the dilute mean-field homogenization scheme in order to derive easily and with low computational effort - without recourse to numerical inversion of the Laplace transform - the effective creep function of a microcracked non-aging viscoelastic mortar. In a second step, the proposed model is based on periodic homogenization accounting for finite thickness of the mortar joints in order to express

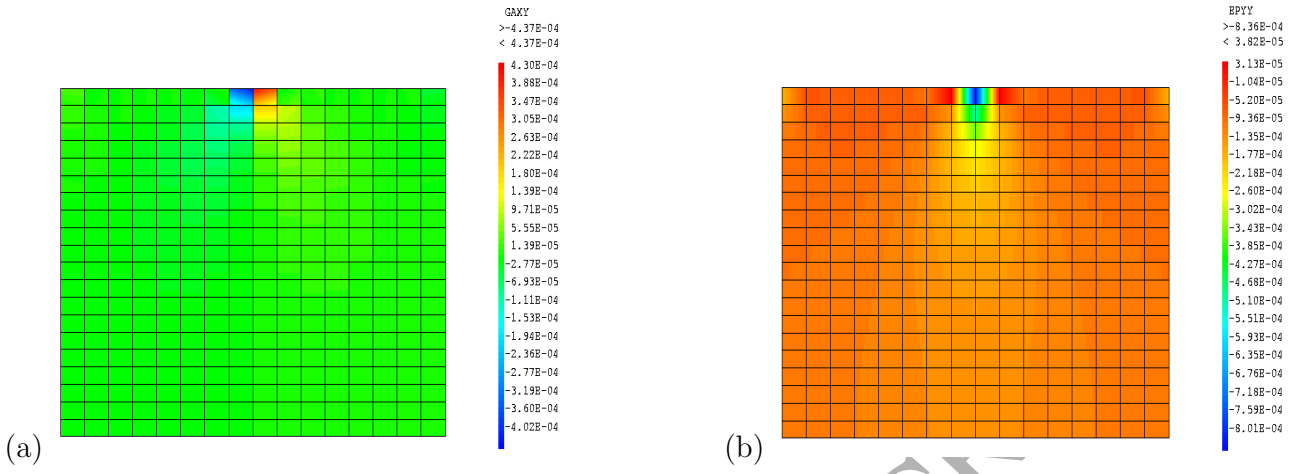

Figure 11: *BC−2 boundary conditions: MM's model predictions for the map of the strain ε_{xy} (a) and ε_{yy} (b) for: $d_c = 0.15$ and 1000 days. Here crack density $d_c = \dot{d}_c t$ where $\dot{d}_c = 1.5\,10^{-4}/day$.*

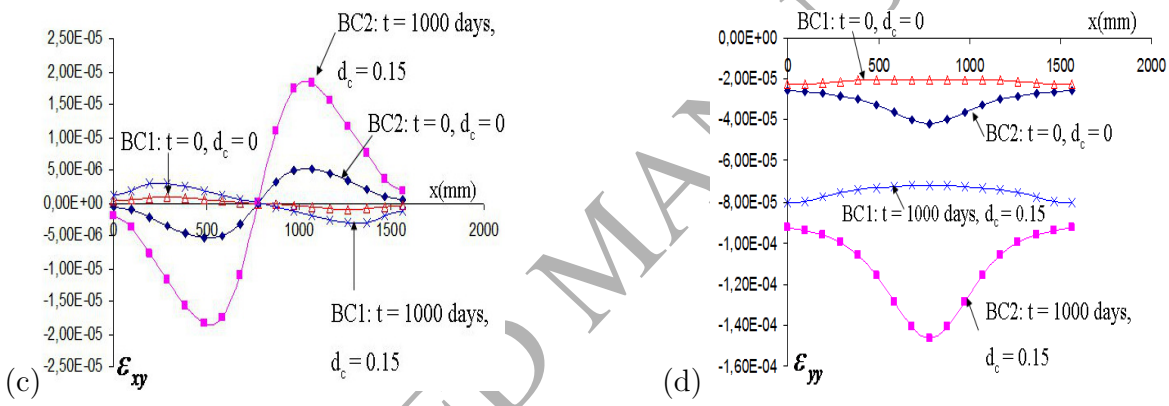

Figure 12: *Boundary condition BC−1 or BC−2: trends in ε_{xy} (a) and ε_{yy} (b) at the panel section A-A for the Modified Maxwell's model at times $t = 0$ with $d_c = 0$ and $t = 1000$ days with $d_c = 0.15$. Here crack density $d_c = \dot{d}_c t$ where $\dot{d}_c = 1.5\,10^{-4}/day$.*

explicitly the effective orthotropic behaviour of the microcracked viscoelastic masonry cell as function of the damage parameter. As a first application, these properties are used to simulate the local behaviour of a viscoelastic loaded (compressed) masonry wall with linear elastic or quasi-rigid bricks. This model allows then the prediction and localization of mostly stressed and deformed areas in a loaded masonry wall or structure. Moreover, the effects of the damage parameter - crack density d_c - and the ratio between the mortar's and bricks stiffness at short and long terms can be assessed. At this stage, this study demonstrates that unlike the proposed MM's model which estimates well the creep of masonry at short to long terms, the relevance of this version of the Burgers model is limited to mortars with too high Maxwell's relaxation times ($\tau_M \geq 10^7(s)$) otherwise it predicts vanishing

stiffness at short and medium terms and exaggerated local strains. At last, this study should be improved on by accounting for creep of bricks which often occurs under high temperatures. More complex loadings and/or a masonry structure (an assembly of walls) could also be considered and simulated using the proposed model. It could be more rigorous to account for interactions between microcracks using the Mori-Tanaka or Ponte-Castañeda & Willis (PCW) homogenization models, to include crack density evolution law and damage rate similar to those proposed in [34, 46, 35, 47]. These perspectives will be investigated in future works.

References

[1] Andreev, K., Sinnema, S., Rekik, A., Allaoui S., Blond E., Gasser A., Compressive behaviour of dry joints in refractory ceramic masonry. Construction and Building Materials (2012) 34, 402–408.

[2] Andreev K., Zinngrebe E., Heijboer W., Compressive behaviour of ACS torpedo bricks, 11^{th} Biennial Worldwide Conference on Unified International Technical Conference Refractories, UNITECR (2009), Salvador (Brazil)

[3] Andreev K., Boursin M., Laurent A., Zinngrebe E., Put P., Sinnema S., Compressive fatigue behaviour of refractories with carbonaceous binders, Journal of the European Ceramic Society 34 (2014) 523–531

[4] Bornert, M., Bretheau, T., Gilormini, P., Homogénéisation en mécanique des matériaux, Tome 1 : Matériaux aléatoires élastiques et milieux périodiques, (2001) Hermes science.

[5] Beurthey, S., Zaoui, A., Structural morphology and relaxation spectra of viscoelastic heterogeneous materials. European Journal of Mechanics A/Solids (2000) 19, 1–16.

[6] Binda L., Gatti G., Mangano G., Poggi C., Sacchi-Landriani G., The collapse of civic tower of Pavia, Masonry International, (1992) 6(1), 11–20

[7] La Borderie C., Berthaud Y., Pijaudier-Cabot G., Crack closure effect in continuum damage mechanics: numerical implementation, in Proc. 2nd Int. Conf. On Computer Aided analysis and design of concrete structures, (1990) 975–986, Zell Am See

[8] Brooks J. J., Composite modeling of masonry deformation, Materials & Structures, 23, 241–251 (1990)

[9] Brooks J. J., Bingel P. R., Creep of masonry under varying stress, Proceeding of the 10th International Brick/Block masonry Conference, Calgary, Alta 5–7 July 1994. Masonry Council of Canada, University of Calgary, Calgary, Alta 749–756

[10] Budiansky B., O′Connell R., Elastic moduli of a cracked solid. Int. J. Solids Struct., (12), 81-97, (1976)

[11] Cecchi, A., Rizzi, N. L., Heterogeneous material: a mixed homogenization rigidification technique. International Journal of Solids and Structures (2001) 38 (1), 29-36.

[12] Cecchi A., Taliercio A. , A comparison between numerical and analytical homogenized models for visco-elastic brickwork, XXI Congresso AIMETA Associazione Italiana di Meccanica Teoricae Applicata, (Torino, Italy), 1-10, (2013)

[13] Cecchi A., Barbieri, A. , Homogenisation procedure to evaluate the effectiveness of masonry strengthening by CFRP repointing technique, Applied and Theoretical Mechanics, 1 (3), (2008)

[14] Cecchi, A., Sab, K., Out of plane model for heterogeneous periodic materials: the case of masonry. European Journal of Mechanics A/Solids (2002) 21, 715-745.

[15] Cecchi, A., Tralli, A., A homogenized viscoelastic model for masonry structures. International Journal of Solids and Structures (2012) 49, 1485–1496.

[16] Chan K. S., Bodner S. R., Fossum A. F., Munson D.E., A constitutive model for inelastic flow and damage evolution in solids under triaxial compression, Mechanics of Materials 14, 1–14, (1992)

[17] Choi, K. K., Lissel, S. L., Taha, M. M. R., Rheological modelling of masonry creep. Canadian Journal of Civil Engineering (2007) 34, 1506-1517.

[18] Cost, T. L., Becker, E. B., A multidata method of approximate laplace transform inversion. Int. J. Num. Meth. Engng. (1970) 2, 207–219

[19] de Felice, G., Metodi di omogeneizzazione per sistemi regolari di corpi rigidi. Proc. Aimeta Napoli (1995), 193-198.

[20] de Felice, G., Détermination des coefficients d'élasticité de la maçonnerie par une méthode d'homogénéisation. Actes du 12ème Congrès Français de Mécanique. Vol. 1. Strasbourg (1995), 393-396.

[21] Deudé V., Dormieux L., Kondo D., Pensée V., Propriétés élastiques non linéaires d'un milieu mésofissuré. Comptes Rendus Mécanique (2002) 330 (8), 587–592.

[22] Dormieux L., Kondo D., Stress-based estimates and bounds of effective elastic properties: the case of cracked media with unilateral effects. Computational Materials Science (2009) 46 (1), 173–179.

[23] Dormieux L., Kondo D., Ulm F.-J., MicroporoMechanics, John Wiley & Sons, 2006.

[24] Dufferene L., Gy R., Viscoelastic constants of a soda-lime silica glass, J. Non-Cryst. Solids 211 (1–2) (1997) 30–38

[25] Ferber M. K., Weresczak A. A., Hemrick J. G., Compressive creep and thermo-physical performance of refractory materials. In: Final Technical Report of Oak Ridge National Laboratory (2006)

[26] Jin S., Harmuth H., Gruber D., Compressive creep testing of refractories at elevated loads - Device, material law and evaluation techniques, Journal of the European Ceramic Society, 34, 4037–4042 (2014)

[27] Huy Duong, B., Mécanique de la rupture fragile. Édition Masson, (1978).

[28] Ignoul, S., Schueremans, L., Tack, J., Swinnen, L., Feytons, S., Binda, L., Gemert, D. V., Balen, K. V., Creep behaviour of masonry structures - failure prediction based on a rheological model and laboratory tests. Structural Analysis of Historical Constructions (2007), Conference, New Delhi.

[29] Klarbring, A., Derivation of model of adhesively bounded joints by the asymptotic expansion method. International Journal of Engineering Science (1991) 29, 493-512.

[30] Koushik B., Georg R., Fritz A., Creep and visco-elastic behaviour of LPS-SiC sintered with Lu_2O_3-AlN additive, Materials Chemistry and Physics 104 (2007) 10-17.

[31] Luciano, R., Sacco, E., Homogenization technique and damage model for old masonry material. International Journal of Solids and Structures (1997) 24, 3191–3208.

[32] Nedjar, B., Le Roy, R., An approach to the modeling of viscoelastic damage: application to the long-term creep of gypsum rock materials. International Journal for Numerical and Analytical Methods in Geomechanics (2013), 37, 1066–1078.

[33] Nguyen T. T. N., Approche multi-échelles pour des maçonneries viscoélastiques. PhD University of Orléans, France (2015).

[34] Papa E., Taliercio A., A visco-damage model for brittle materials under monotonic and sustained stresses, International journal for numerical and analytical methods in geomechanics, 29 (3), 287–310 (2005)

[35] Papa E., Taliercio A., Modeling of the long-term behaviour of historical masonry towers, Chapter 7 in Book: Learning from Failure: Long-term Behaviour of Heavy Masonry Structures, 153–173 (2008), published by Binda L.

[36] Nguyen, S. T., Propagation de fissures et endommagement par microfissures dans un milieu viscoélastique linéaire non veillissant. PhD, University Paris-Est, France (2010).

[37] Nguyen S. T., Dormieux L., Le Pape, Y., Sanahuja, J., A Burger Model for the Effective Behavior of a Microcracked Viscoelastic Solid, International Journal of Damage Mechanics, 20 (8), 1116–1129, (2011)

[38] Nguyen, S. T., Jeannin, L., Dormieux, L., Renard, F., Fracturing of viscoelastic geomaterials and application to sedimentary layered rocks. Mechanics Research Communications (2013) 49, 50–56.

[39] S.T. Nguyen, Generalized Kelvin model for micro-cracked viscoelastic materials, Engineering Fracture Mechanics 127 (2014) 226-234

[40] Rekik, A., Brenner, R., Optimization of the collocation inversion method for the linear viscoelastic homogenization. Mechanics Research Communications (2011), 38, 305–308.

[41] Sacco, E., A nonlinear homogenization procedure for periodic masonry. European Journal of Mechanics - A/Solids (2009) 28, 209–222.

[42] Schapery, R. A., Approximate methods of transform inversion for viscoelastic stress analysis. Proc. U.S. Nat. Congr. Appl. Mech. ASME 4th. Vol. 2. (1962) 1075–1085.

[43] Shrive N. G. , Sayed-Ahmed E. Y. , Tilleman D., Creep analysis of clay masonry assemblages, Canadian Journal of Civil Engineering (1997) 367–397

[44] Shrive N. G. , Huizier A., Letter to the Editor, The masonry Society Journal, 9(2), 4 (1991)

[45] Taliercio A., Closed-form expressions for the macroscopic in-plane elastic and creep coefficients of brick masonry, International Journal of Solids and Structures 51 (2014) 2949-2963

[46] Verstrynge, E., Schueremans, L., Dionys, D.V., Time-dependent mechanical behaviour of lime-mortar masonry. Materials and Structures (2011) 44, 29–42.

[47] Verstrynge, E., Ignoul S., Schueremans L., Gemert Van D., Modelling of damage accumulation in masonry subjected to a long-term compressive load, Book: Structural analysis of histric construction, Dina d'ayala & Enrico Fodde editors, CRC Press (2008), 525–532.

A. Burgers model (Bu): microcracked state

An approximation of the Burgers' type for the creep function of a microcracked non-aging linear viscoelastic mortar with a matrix following the Burgers' rheology is

$$J^{app}_{Bu}(t,dc) = \frac{1}{9k_M(d_c)} + \frac{1}{3\mu_M(d_c)} + \left(\frac{1}{3\eta^s_M(d_c)} + \frac{2}{3\eta^d_M(d_c)}\right)t + \frac{(1-e^{-t/\tau^s_K(d_c)})}{9k_K(d_c)} + \frac{(1-e^{-t/\tau^d_K(d_c)})}{3\mu_K(d_c)} \quad (53)$$

where

$$\begin{aligned} \frac{1}{\mu_M(d_c)} &= \frac{1+M^e_M d_c}{\mu^e_M}, & \frac{1}{\mu_K(d_c)} &= \frac{1+M^e_K d_c}{\mu^e_K} \\ \frac{1}{\eta^d_M(d_c)} &= \frac{1+M^v_M d_c}{\eta^d_M}, & \frac{1}{\eta^d_K(d_c)} &= \frac{1+M^v_K d_c}{\eta^d_K} \end{aligned} \quad (54)$$

with $M^e_M = M^\infty_0$, $M^v_M = M^0_0$, $M^e_K = M^0_0 + \frac{2\mu_K}{\eta^d_M}M^0_1 - \frac{\mu_K}{\mu_M}(M^e_M - M^0_0)$ and $M^v_K = M^0_\infty + \frac{\eta^d_K}{2\mu_M}M^{-1}_\infty - \frac{\eta^d_K}{\eta^d_M}(M^v_M - M^0_\infty)$, and

$$\begin{aligned} \frac{1}{k_M(d_c)} &= \frac{1+Q^e_M d_c}{k_M}, & \frac{1}{k_K(d_c)} &= \frac{1+Q^e_K d_c}{k_K}, \\ \frac{1}{\eta^s_M(d_c)} &= \frac{1+Q^v_M d_c}{\eta^s_M}, & \frac{1}{\eta^s_K(d_c)} &= \frac{1+Q^v_K d_c}{\eta^s_K} \end{aligned} \quad (55)$$

with $Q^e_M = Q^\infty_0$, $Q^v_M = Q^0_0$, $Q^e_K = Q^0_0 + 3\frac{k_K}{\eta^s_M}Q^1_0 - \frac{k_K}{k_M}(Q^e_M - Q^0_0)$ and $Q^v_K = Q^\infty_0 + \frac{\eta^s_K}{3k_M}Q^{-1}_\infty - \frac{\eta^s_K}{\eta^s_M}(Q^v_M - Q^\infty_0)$

where the identified parameters of the Burgers model at the vicinity of 0 and ∞ are respectively the

following

$$
\begin{aligned}
Q_0^0 &= \frac{16\eta_M^s(2\eta_M^d+\eta_M^s)}{9\eta_M^d(\eta_M^d+2\eta_M^s)},\\
Q_0^1 &= \frac{16(\eta_M^s(\eta_M^{d^2}+\eta_M^s\eta_M^d+\eta_M^{s^2})(-2\eta_M^s(k_K+k_M^e)\mu_K\mu_M^e+3\eta_M^d k_K k_M^e(\mu_K+\mu_M^e))}{27\eta_M^d(\eta_M^d+2\eta_M^s)^2 k_K k_M^e\mu_K\mu_M^e}\\
M_0^0 &= \frac{32(2\eta_M^d+\eta_M^s)(2\eta_M^d+3\eta_M^s)}{45(\eta_M^d+\eta_M^s)(\eta_M^d+2\eta_M^s)}\\
M_0^1 &= \frac{16(\eta_M^s\eta_M^d(4{\eta_M^d}^2+10\eta_M^d\eta_M^s+7{\eta_M^s}^2)(2\eta_M^s(k_K+k_M^e)\mu_K\mu_M^e-3\eta_M^d k_K k_M(\mu_K+\mu_M)))}{135((\eta_M^d+\eta_M^s)^2(\eta_M^d+2\eta_M^s)^2)k_K k_M\mu_k\mu_M}
\end{aligned}
\tag{56}
$$

and

$$
\begin{aligned}
Q_\infty^0 &= \frac{4}{3}k_M^e\left(\frac{1}{\mu_M^e}+\frac{3}{3k_M^e+\mu_M^e}\right)\\
Q_\infty^1 &= -\frac{4(k_M^e(3\eta_K^d\eta_M^d(\eta_K^s+\eta_M^s)k_M^e-2\eta_K^s(\eta_K^d+\eta_M^d)\eta_M^s\mu_M^e)(9{k_M^e}^2+6k_M^e\mu_M^e+4{\mu_M^e}^2)))}{3(\eta_K^d\eta_K^s\eta_M^d\eta_M^s\mu_M^e(3k_M^e+\mu_M^e)^2)}\\
M_\infty^0 &= \frac{16(3k_M^e+4\mu_M^e)(9k_M^e+4\mu_M^e)}{45(3k_M^e+\mu_M^e)(3k_M^e+2\mu_M^e)}\\
M_\infty^1 &= \frac{16k_M^e\mu_M^e(3\eta_K^d\eta_M^d(\eta_K^s+\eta_M^s)k_M^e-2\eta_K^s(\eta_K^d+\eta_M^d)\eta_M^s\mu_M^e)(63{k_M^e}^2+60k_M^e\mu_M^e+16{\mu_M^e}^2)}{15\eta_K^d\eta_K^s\eta_M^d\eta_M^s(3k_M^e+\mu_M^e)^2(3k_M^e+2\mu_M^e)^2}
\end{aligned}
\tag{57}
$$

If spherical and deviatoric relaxtation times are equal ($\tau_i^s=\tau_i^d=\tau_i$ where $i=M$ or K), then the effective creep function (53) reads

$$
J_{Bu}(t)=\frac{1}{E_M(d_c)}+\frac{t}{E_M(d_c)\tau_M(d_c)}+\frac{1}{E_K(d_c)}(1-e^{-\frac{t}{\tau_K(d_c)}}) \tag{58}
$$

where $\frac{1}{E_M(d_c)}=\frac{1}{9k_M(d_c)}+\frac{1}{3\mu_M(d_c)}=\frac{1}{9k_M}+\frac{1}{3\mu_M}+(\frac{Q_M^e}{9k_M}+\frac{M_M^e}{3\mu_M})d_c$ and $\tau_M^s(d_c)=\tau_M^s\frac{1+Q_M^e d_c}{1+Q_M^v d_c}$. Recall that relaxation times at undamaged state are the following: $\tau_M^s=\frac{\eta_M^s}{3k_M}$, $\tau_M^d=\frac{\eta_M^d}{2\mu_M}$, $\tau_K^s=\frac{\eta_K^s}{3k_K}$ and $\tau_K^d=\frac{\eta_K^d}{2\mu_K}$.

B. Elastic bricks: effect of the material parameter β and the crack density

B.1. Constant crack density

Mortar	t (days)	d_c	$\tilde{E}_{tt}$ (MPa)	$\tilde{E}_{nn}$ (MPa)	$\tilde{\nu}_{tn}$	$\tilde{\nu}_{nt}$	$\tilde{\mu}_{tn}$ (MPa)
Burgers model	0	0	53286.	15351.7	0.0545	0.0157	4538.53
	25	0.1	2554.32	129.099	0.007	0	169.355
	100	0.1	684.108	31.76	0.002	0.0	44.978
	1000	0	82.304	3.715	0	0	5.396
	1000	0.1	69.90	3.15	0	0	4.583
Modified Maxwell	0	0	80569.6	31283.2	0.144	0.056	11743
	1000	0	48549.8	12906.9	0.0868	0.0230	4760.92
	1000	0.1	43838.88	11138.	0.0784	0.0199	4101.52
Absolute error E_r (%)			45.6	64.4	45.5	64.4	65

Table 5: Cecchi & Tralli's extension model: effective properties of a periodic masonry cell with elastic bricks ($E_b = 20E_m$) and hybrid viscoelastic mortar [28]

Mortar	t (days)	d_c	$\tilde{E}_{tt}$ (MPa)	$\tilde{E}_{nn}$ (MPa)	$\tilde{\nu}_{tn}$	$\tilde{\nu}_{nt}$	$\tilde{\mu}_{tn}$ (MPa)
Modified Maxwell model	0	0	79579.9	30169.8	0.142	0.054	11721.8
	≥ 100	0	47512.4	12349.7	0.085	0.0220	4750.74
	≥ 100	0.1	42844.1	10648.9	0.0766	0.0190	4092.63
Maxi. absolute error E_r'(%)			2.32	4.6	2.35	4.7	0.02

Table 6: Cecchi & Taliercio's extension model: effective properties of a periodic masonry cell with elastic bricks ($E_b = 20E_m$) and hybrid viscoelastic mortar [28]

Mortar	t (days)	d_c	$\tilde{E}_{tt}$ (MPa)	$\tilde{E}_{nn}$ (MPa)	$\tilde{\nu}_{tn}$	$\tilde{\nu}_{nt}$	$\tilde{\mu}_{tn}$ (MPa)
Burgers model	0	0	78902.7	14538.9	0.048	0.009	6253.53
	25	0.1	2595.3	123.957	0.00378	0.0001	171.106
	1000	0	82.346	3.709	0	0	5.398
	1000	0.1	69.936	3.149	0	0	4.584
Modified Maxwell	0	0	119811	35860.3	0.107	0.032	13291.1
	≥ 100	0	60487.5	13625.	0.0540	0.012	4996.888
	≥ 1000	0.1	53345.43	11668.6	0.0477	0.0104	4275.45
Absolute error E_r (%)			55.5	67.5	55.4	67.5	67.8

Table 7: Cecchi & Tralli's extension model: effective properties of a periodic masonry cell with elastic bricks ($E_b = 40E_m$) and hybrid viscoelastic mortar [28]

Mortar	t (days)	dc	$\tilde{E}_{tt}$ (MPa)	$\tilde{E}_{nn}$ (MPa)	$\tilde{\nu}_{tn}$	$\tilde{\nu}_{nt}$	$\tilde{\mu}_{tn}$ (MPa)
Modified Maxwell model	0	0	117634.	34387.1	0.105	0.030	13263.9
	≥ 100	0	58885.5	13002.4	0.052	0.0116	4985.678
	≥ 100	0.1	51879.7	11130.7	0.046	0.010	4265.79
Maxi. absolute error $E_r^{'}$ (%)			2.82	4.83	2.17	4	0.02

Table 8: Cecchi & Taliercio's extension model: effective properties of a periodic masonry cell with elastic bricks ($E_b = 40E_m$) and hybrid viscoelastic mortar [28]

B.2. Time-dependent crack density

Mortar	t (days)	d_c	$\tilde{E}_{tt}$ (MPa)	$\tilde{E}_{nn}$ (MPa)	$\tilde{\nu}_{tn}$	$\tilde{\nu}_{nt}$	$\tilde{\mu}_{tn}$ (MPa)
Modified Maxwell model	0	0	79579.9	30169.8	0.142	0.054	11721.8
	1	$1.5\ 10^{-4}$	60351.7	17945.9	0.107	0.032	6925.02
	5	$7\ 10^{-4}$	48273.4	12641.8	0.086	0.0226	4863.91
	40	$6\ 10^{-3}$	47204.8	12232.8	0.0844	0.021	4705.5
	100	$1.5\ 10^{-2}$	46751.	12061.7	0.0836	0.0215	4639.23
	500	$7.4\ 10^{-2}$	43934.7	11032.8	0.078	0.019	4241.05
	1000	0.15	40858.1	9969.66	0.073	0.0178	3830.13
	1200	0.2	39744.9	9599.65	0.071	0.017	3687.23

Table 9: Cecchi & Taliercio's extension model: effective properties of a periodic masonry cell with elastic bricks ($E_b = 20E_m$) and hybrid viscoelastic mortar accounting for time-dependent d_c with a constant rate $\dot{d}_c = 1.5\text{x}10^{-4}$/day.

Mortar	t (days)	dc	$\tilde{E}_{tt}$ (MPa)	$\tilde{E}_{nn}$ (MPa)	$\tilde{\nu}_{tn}$	$\tilde{\nu}_{nt}$	$\tilde{\mu}_{tn}$ (MPa)
Modified Maxwell model	0	0	117634.	34387.1	0.105	0.030	13263.9
	1	$1.5\ 10^{-4}$	60058.9	13326.6	0.053	0.012	13326.6
	5	$7\ 10^{-4}$	58413.9	12873.	0.052	0.0116	4935.87
	40	$6\ 10^{-3}$	58413.9	12873.	0.052	0.052	4935.87
	100	$1.5\ 10^{-2}$	57720.4	12683.6	0.0516	0.0113	4863.01
	500	$7.4\ 10^{-2}$	53487.4	11550.8	0.0478	0.010	4427.29
	1000	0.15	48995.8	10390.8	0.043	0	3981.39
	1200	0.2	47403.6	9989.47	0.042	0	3827.2

Table 10: Cecchi & Taliercio's extension model: effective properties of a periodic masonry cell with elastic bricks ($E_b = 40E_m$) and hybrid viscoelastic mortar accounting for time-dependent d_c with a constant rate $\dot{d}_c = 1.5\text{x}10^{-4}$/day.

C. Long-term characteristic times and corresponding effective properties

E_M (MPa)	τ_M (s)	E_R (MPa)	τ_R (s)	ν_m
3500	690000	30000	7500	0.2

Table 11: Elastic and viscous moduli of tested specimens from Pavia Tower [35]

E_M (MPa)	τ_M (s)	E_R (MPa)	τ_R (s)	ν_m
4000	2x10^8	2112	300000	0.29

Table 12: Elastic and viscous moduli of hybrid mortar at long-term [47]

Mortar: rheological model	t (days)	d_c	$\tilde{E}_{tt}$ (MPa)	$\tilde{E}_{nn}$ (MPa)	$\tilde{\nu}_{tn}$	$\tilde{\nu}_{nt}$	$\tilde{\mu}_{tn}$ (MPa)
Burgers	0	0	66946.1	19569.9	0.105	0.030	7548.55
	1	$1.5\,10^{-4}$	59434.2	16195.5	0.093	0.025	6236.67
	5	$7\,10^{-4}$	48204.6	11926.1	0.075	0.0118	4583.06
	40	$6\,10^{-3}$	18051.84	3580.9	0.028	0.0056	1370.53
	100	$1.5\,10^{-2}$	8599.9	1606.15	0.0135	0.002	614.14
	500	$7.4\,10^{-2}$	1754.31	314.32	0.0027	0	120.11
	1000	0.15	797.30	142.	0.0012	0	54.27

Table 13: Cecchi & Taliercio's extension model: effective properties of a periodic masonry cell with elastic bricks ($E_b = 40E_m$) and long-term characteristic time viscoelastic mortar (similar to those of tested specimens from the Pavia Tower [35]) accounting for time-dependent d_c with a constant rate $\dot{d}_c = 1.5\text{x}10^{-4}$/day.

Mortar	t (days)	dc	$\tilde{E}_{tt}$ (MPa)	$\tilde{E}_{nn}$ (MPa)	$\tilde{\nu}_{tn}$	$\tilde{\nu}_{nt}$	$\tilde{\mu}_{tn}$ (MPa)
Burgers model	0	0	75875.3	22365.6	0.137	0.040	8177.6
	1	$1.5\ 10^{-4}$	60718.9	15880.3	0.11	0.028	5790.89
	5	$7\ 10^{-4}$	43045.6	9950.05	0.078	0.018	3619.56
	40	$6\ 10^{-3}$	37547.5	8376.39	0.068	0.015	3045.14
	100	$1.5\ 10^{-2}$	36856.9	8186.47	0.066	0.0148	2975.87
	500	$7.4\ 10^{-2}$	32678.9	7071.83	0.06	0.013	2569.51
	1000	0.15	28339.1	5973.14	0.05	0.01	2169.34
	1200	0.2	26831.	5604.61	0.038	0.01	2035.19

Table 14: Cecchi & Taliercio's extension model: effective properties of a periodic masonry cell with elastic bricks ($E_b = 40E_m$) and long-term characteristic time viscoelastic hybrid mortar [47] accounting for time-dependent d_c with a constant rate $\dot{d}_c = 1.5\text{x}10^{-4}$/day.

Mortar	t (days)	d_c	$\tilde{E}_{tt}$ (MPa)	$\tilde{E}_{nn}$ (MPa)	$\tilde{\nu}_{tn}$	$\tilde{\nu}_{nt}$	$\tilde{\mu}_{tn}$ (MPa)
Modified Maxwell model	0	0	117202.	34174.6	0.096	0.028	13392.3
	1	$1.5\ 10^{-4}$	117169.	34158.7	0.096	0.028	13386.
	5	$7\ 10^{-4}$	117036.	34095.	0.095	0.027	13360.8
	40	$6\ 10^{-3}$	115886.	33545.1	0.094	0.027	13143.3
	100	$1.5\ 10^{-2}$	113942.	32632.	0.093	0.026	12782.2
	500	$7.4\ 10^{-2}$	101894.	27378.5	0.083	0.022	10708.5
	1000	0.15	88940.	22408.9	0.072	0.018	8752.45
	1200	0.2	84363.4	20798.	0.069	0.017	8119.59

Table 15: Cecchi & Taliercio's extension model: effective properties of a periodic masonry cell with elastic bricks ($E_b = 40E_m$) and long-term characteristic time viscoelastic hybrid mortar [47] accounting for time-dependent d_c with a constant rate $\dot{d}_c = 1.5\text{x}10^{-4}$/day.

Mortar	t (days)	dc	$\tilde{E}_{tt}$ (MPa)	$\tilde{E}_{nn}$ (MPa)	$\tilde{\nu}_{tn}$	$\tilde{\nu}_{nt}$	$\tilde{\mu}_{tn}$ (MPa)
Modified Maxwell model	0	0	642386.	187312.	0.096	0.028	73403.7
	1	$1.5\ 10^{-4}$	638185.	184770.	0.095	0.027	72398.1
	5	$7\ 10^{-4}$	625619.	179369..	0.093	0.026	70262.2
	40	$6\ 10^{-3}$	602474.	168831.	0.09	0.025	66098.4
	100	$1.5\ 10^{-2}$	596888.	166359.	0.09	0.024	65122.3
	500	$7.4\ 10^{-2}$	564396.	152494.	0.084	0.022	59652.
	1000	0.15	528439.	138106.	0.078	0.02	53983.9
	1200	0.2	515307.	133083.	0.077	0.02	52007.2

Table 16: Cecchi & Taliercio's extension model: effective properties of a periodic masonry cell with elastic bricks ($E_b = 40E_m$) and long-term characteristic time viscoelastic mortar (similar to those of tested specimens from Pavia Tower [35]) accounting for time-dependent d_c with a constant rate $\dot{d}_c = 1.5\text{x}10^{-4}$/day.

D. Validation step for a hybrid mortar

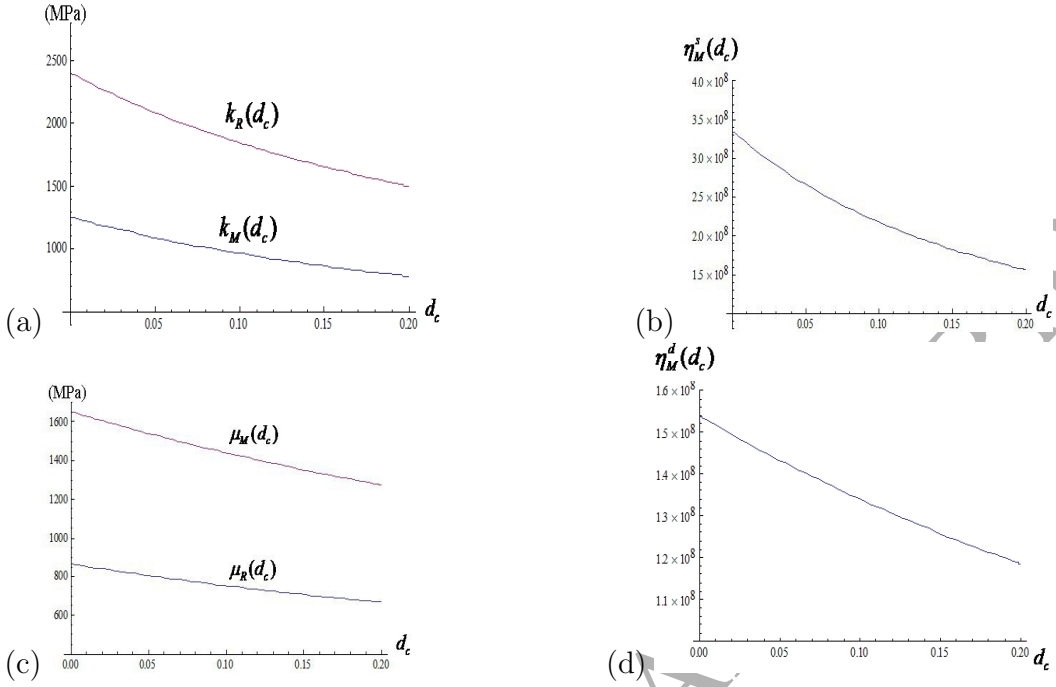

Figure 13: *Mortar following the MM's model: Variation of MM's parameters versus the crack density* d_c.